

Immunothrombotic Dysregulation in COVID-19 Pneumonia is Associated with Respiratory Failure and Coagulopathy

Running Title: Nicolai et al.; Immunothrombosis in COVID-19

Leo Nicolai, et al.

The full author list is available on page 23.

Addresses for Correspondence:

Leo Nicolai, MD
Medizinische Klinik und Poliklinik I
University Hospital Ludwig-Maximilian-University Munich
Marchioninstr. 15 81377
Munich, Germany
Tel: 089-218076505
Email: leo.nicolai@med.uni-muenchen.de



Kami Pekayvaz, MD
Medizinische Klinik und Poliklinik I
University Hospital Ludwig-Maximilian-University Munich
Marchioninstr. 15 81377
Munich, Germany
Tel: 089-2180 76515
Email: kami.pekayvaz@med.uni-muenchen.de

Abstract

Background: SARS-CoV-2 infection causes severe pneumonia (COVID-19), but the mechanisms of subsequent respiratory failure and complicating renal and myocardial involvement are poorly understood. In addition, a systemic prothrombotic phenotype has been reported in COVID-19 patients.

Methods: A total of 62 subjects were included in our study (n=38 patients with RT-PCR confirmed COVID-19 and n=24 non-COVID-19 controls). We performed histopathological assessment of autopsy cases, surface-marker based phenotyping of neutrophils and platelets, and functional assays for platelet, neutrophil functions as well as coagulation tests.

Results: We provide evidence that organ involvement and prothrombotic features in COVID-19 are linked by immunothrombosis. We show that in COVID-19 inflammatory microvascular thrombi are present in the lung, kidney, and heart, containing neutrophil extracellular traps associated with platelets and fibrin. COVID-19 patients also present with neutrophil-platelet aggregates and a distinct neutrophil and platelet activation pattern in blood, which changes with disease severity. Whereas cases of intermediate severity show an exhausted platelet and hyporeactive neutrophil phenotype, severely affected COVID-19 patients are characterized by excessive platelet and neutrophil activation compared to healthy controls and non-COVID-19 pneumonia. Dysregulated immunothrombosis in SARS-CoV-2 pneumonia is linked to both ARDS and systemic hypercoagulability.

Conclusions: Taken together, our data point to immunothrombotic dysregulation as a key marker of disease severity in COVID-19. Further work is necessary to determine the role of immunothrombosis in COVID-19.

Key Words: COVID-19; SARS-CoV-2; thrombosis; platelets; neutrophils; immunothrombosis; NETs; NETosis; coagulopathy; respiratory failure

Non-standard Abbreviations and Acronyms:

ARDS: acute respiratory distress syndrome

COVID-19: Corona Virus Disease 2019

DIC: Disseminated Intravascular Coagulation

ECG: Electrocardiogramm

GFR: Glomerular Filtration Rate

NETosis: neutrophil extracellular trap formation

PMN: Polymorphonuclear Cells

RT-PCR. Reverse Transcriptase Polymerase Chain Reaction

SARS-CoV-2: Severe Acute Respiratory Syndrome Corona Virus 2

Clinical Perspective

What is new?

- Dysregulated platelets and neutrophils cooperate to drive a systemic prothrombotic state in SARS-CoV-2 infection, indicating inflammation as trigger for thrombotic complications frequently observed during COVID-19.
- Microvascular thrombi containing neutrophils, platelets, and Neutrophil Extracellular Traps (NETs) are a hallmark of severe SARS-CoV-2 infection, linking multi-organ failure and systemic hypercoagulability in COVID-19.

What are the clinical implications?

- SARS-CoV-2 infected patients are at increased risk for thrombotic events, making prophylactic anticoagulation and vigilant monitoring for thrombotic complications a central task in management of COVID-19 patients.
- Targeting immunothrombosis or NETosis by modulating platelet-neutrophil interactions could be a valuable therapeutic approach for respiratory failure and thrombotic complications in COVID-19.



Circulation

Introduction

The COVID-19 pandemic is a global health care challenge, with rapid spread, high contagiousness and an approximate case fatality rate of 1.0-2.3%¹⁻⁴. However, due to the lack of specific treatment, therapy has so far mainly been limited to supportive care⁴⁻⁶.

Although acute respiratory distress syndrome (ARDS) is the central feature of disease severity, non-pulmonary organ damage has emerged as an important predictor of mortality⁷. Patients hospitalized for COVID-19 are at high risk for kidney failure and myocardial involvement is common in severe cases, both correlating with poor outcome⁸⁻¹⁰. The underlying mechanisms of COVID-19 pulmonary and non-pulmonary tissue injury are insufficiently understood¹¹.

Preliminary data point to a prothrombotic state in COVID-19 patients¹², with a possible beneficial effect of heparin. However, a thorough analysis of cellular and plasmatic coagulation of affected patients is missing¹³⁻¹⁵. In particular, it is unclear whether and how the inflammatory response to SARS-CoV-2 and its associated coagulopathy are intertwined. Recent evidence from translational and basic research has established the concept of immunothrombosis, a process that integrates innate immunity, platelets and clotting factors to capture and fight invading pathogens but also contributes to inflammation-related tissue damage^{16, 17}.

In this study, we provide first evidence that neutrophils, immunogenic platelets, and a dysregulated coagulation cascade cooperate to propagate immunothrombotic tissue injury in COVID-19, as shown in autopsy specimens and the blood of patients. Our data show distinct neutrophil and platelet activation states and increased plasmatic coagulation in COVID-19, all of which correlate with disease progression. Therefore, immunothrombosis is not only a bystander

in COVID-19 but represents a central pathogenic factor linking respiratory failure and systemic hypercoagulability.

Methods

Cohort

The data that support the findings of this study are available from the corresponding author upon reasonable request. A total of 62 subjects were included in our study (n=38 patients with RT-PCR confirmed COVID-19 and n=24 non-COVID-19 control groups). The study design is outlined in (Fig. Ia-e in the Supplement). Patients with severe pre-existing kidney or liver dysfunction, severe autoimmune diseases, immunosuppression, chronic infection, patients requiring ECMO therapy, with a known coinfection with Influenza or Respiratory Syncytial Virus (RSV) and patients receiving antiplatelet medication were excluded. COVID-19 patients were divided into a group of severe cases requiring intubation and intensive care treatment (CoV_sev, n=18), and a group of intermediate severity (CoV_int, n=20), which were hospitalized and either required no oxygen or received non-invasive supplemental oxygen. Horowitz Indices (paO_2/FiO_2) of CoV_sev patients were directly derived from ventilation parameters. For CoV_int, Horowitz index was calculated from non-invasive oxygen support (FiO_2 approximation) and pulse oximetry (paO_2 approximation)¹⁸.

Flow cytometric phenotyping and platelet/coagulation testing

31 patients with COVID-19, 5 patients with non-COVID-19 pneumonia and 10 age-matched control patients without pulmonary pathology were included for flow cytometry, ROTEM and PFA analyses. Baseline characteristics of the flow cytometric phenotyping and platelet/coagulation testing cohorts are detailed in Table I in the Supplement. Flow cytometric

analysis was performed with blood from 11 intermediate and 5 severe COVID-19 patients, whereas platelet function testing, whole blood impedance blood aggregometry, and rotational thrombelastometry were performed on blood from 9 intermediate and 8 severe COVID-19 patients, with an overlap of two severe COVID-19 patients. To avoid batch effects, principle component analysis, t-SNE based dimension reduction and automated clustering was performed in n=7 controls, n=4 non-COVID-19 pneumonia, n=5 CoV_sev and n=11 CoV_int patients sampled and analyzed within 10 days.

Histopathological assessment

One patient, aged 91 years, showed a typical disease course, declined intensive care treatment and was autopsied after developing progressive ARDS and succumbing to the infection on the seventh day after hospitalization (see details in Results and Fig. 1a-b). For quantification of immunothrombosis /NETosis, lung specimens from 4 additional deceased patients with RT-PCR confirmed COVID-19 (Age (Median= 78, IQR 69-86); Male (N=3, 60%)) were included, as well as five patients, who had died from cardiovascular events without lung involvement. One lung autopsy specimen was from a deceased COVID-19 patient who was also included in the flow cytometric phenotyping as a severe COVID-19 patient.

In vitro assays

We used peripheral blood from 3 additional RT-PCR confirmed COVID-19 patients requiring ICU care (Age (Median=77, IQR= 67-81); Male (N=1, 33%)) and 5 healthy control patients, with an overlap of one control patient with the flow cytometric analysis, for in-vitro analysis of platelet activation assay neutrophil isolation, assessment of steady-state activation and induction of NETosis with platelet-rich plasma.

In accordance with the Declaration of Helsinki, and with the approval of the Ethics Committee of Ludwig-Maximilian-University Munich, informed consent of the patients or their guardians was obtained. COVID-19 patients are part of the COVID-19 Registry of the LMU University Hospital Munich (CORKUM, WHO trial ID DRKS00021225). Pseudonymized data was used for analysis, the study was approved by the ethics committee of LMU Munich (No: 20-245 and 19-274).

Histopathology

Histopathology and immunofluorescence stainings were performed on paraffin-embedded heart, lung and kidney specimens of the autopsy specimen described in Figure 1. Hematoxylin-Eosin (HE) and Van Gieson's (EvG) stainings were performed as previously described¹⁹. For immunofluorescence staining, specimens were deparaffinized and subsequently stained using a published protocol¹⁹. For histological quantification we used 4 additional lung autopsy specimens from COVID-19 deceased patients, and 5 lung autopsy specimens of patients deceased from cardiovascular events without lung involvement. Used antibodies were anti-Myeloperoxidase (MPO), anti-citrullinated histone H3, anti-fibrinogen, anti-CD42b and Hoechst 33342 for immunofluorescences, as well as anti-Fibrin and anti-CD42b for immunohistochemistry. Slides were visualized using either Airyscan technology (Zeiss LSM 880), epifluorescence microscopy (Zeiss) or Vectra Polaris system. The 3D reconstruction was rendered with Imaris. For quantification of NETs and microthrombi, blood vessels were defined as tubular or circular enclosed structures with DAPI-positive endothelial lining and visible elastica interna as well as lack of ciliated epithelium and a lack of obvious communication with alveoli. Intravascular cells were regarded as neutrophils if they stained positive for DAPI and MPO. NETs were defined as extracellular structures adjacent to MPO-positive neutrophils that

stained MPO⁺ and citH3⁺ as well as DAPI^{int/high}. Vessels were considered to contain immunothrombotic occlusions if there was a (partial) occlusion of the vessel lumen that stained positive for a network of fibrinogen, neutrophils (MPO) and platelets (CD41) (see Fig. IIa in the Supplement). The mean of 3 high power fields for each patient without massive lung damage or hepatization was used. Quantification was performed with ImageJ v2.0.0-rc-69.

Platelet and neutrophil phenotyping

Blood samples were obtained either from a peripheral vein or an arterial line. 2 ml of patient blood was mixed with a Lysing-PFA-Fixation solution containing 300 μ l Heparin, 15.7 ml distilled water and 2 ml FACS Lysing Solution 10x (BD Biosciences), containing formaldehyde and diethylene glycol. Blood was incubated for at least one hour to ensure complete virus inactivation and lysis of the red blood cells. Lysates were then centrifuged (400 G/7 min) and the resulting pellets were resuspended in 400 μ l PBS containing 0.5% BSA. 50 μ l of the suspension was incubated with 50 μ l of the antibody panel (Table II in the Supplement) for 20 minutes at room temperature. Measurements were performed on a BD LSRFortessa Flow Cytometer.

Analysis was performed using FlowJo Software (FlowJo v. 10.6.1, BD).

After down-sampling twice with Downsample v3 plugin and two concatenation steps, t-Distributed Stochastic Neighbor Embedding (t-SNE) of an equal and representative number of cells per group was performed using the t-SNE FlowJo plugin. Subpopulations detection was performed by applying the Phenograph algorithm (Phenograph Plugin for FlowJo)²⁰, the resulting Phenograph clustering was then used to assign the neutrophil and platelet subpopulations. The principal component analysis and heatmaps were created using the ClustVis algorithm²¹. All mean fluorescence intensities (MFIs) reported are relative MFIs (percent of maximum expression for particular marker) in arbitrary units (A.U.). ClustVis heatmap

clustering was performed via correlation distance, average clustering with tightest cluster first for rows and Manhattan distance, complete clustering and higher mean value first for columns or with no clustering for columns. Hyporeactive neutrophils were defined as decreased expression of naïve-neutrophil marker L-selectin (CD62L), adhesion receptors CD11b and CD49d as well as FcγRIII (CD16). Exhausted platelets were defined as platelets that show a low expression of CD40L, as well as low activation marker exposure.

In-vitro assay

Blood from 3 COVID-19 patients with severe disease (CoV_sev) and 5 control donors (Ctrl) was used for in-vitro assays. Flow cytometric measurements were performed on a BD LSRFortessa Flow Cytometer. Analysis was performed using FlowJo Software (FlowJo v. 10.6.1, BD). Histological analysis was performed with ImageJ v2.0.0-rc-69.



Platelet activation assay

Human platelets were isolated from citrated whole blood as described previously²², labeled antibodies against CD62P (BioLegend, Cat. 304925) and PAC-1 (BioLegend, 362806) and subsequently exposed to Thrombin (0.01 and 0.1 U/ml), Convulxin (0.1 µg/ml), ADP (10 µM), Collagen (20 µg/ml) or NaCl (Unstimulated) for 20 min at RT. After fixation with paraformaldehyde (PFA, 1% final concentration), degranulation and integrin IIbIIIa activation were assessed by measuring mean fluorescent intensities of CD62P and PAC-1.

Neutrophil isolation and assessment of steady-state activation

Whole blood was drawn from CoV_sev patients (n = 3) and healthy donors (n = 5) into EDTA-containing vials. Neutrophil granulocytes were isolated using magnetic beads (EasySep® Direct Human Neutrophil Isolation Kit, Stemcell Technologies, Cat. #19666) according to manufacturer's instructions. Isolated neutrophils were subsequently seeded onto Ibidi® µ-Slides

(VI 0.4) coated with poly-L lysine (Sigma) by brief centrifugation (40G, 5 min), washed with PBS three times and then fixed with 1% PFA (10 min). Cells were permeabilized (0.5% triton X-100, 10 min) and stained with anti-myeloperoxidase (MPO, R&D Systems AF3667), anti-citrullinated histone H3 (abcam ab5103) and Hoechst dye for 30 min. Cells were visualized by immunofluorescence microscopy (6 fields of view at 40x magnification per replicate), and the number of activated neutrophils defined by citr. H3-positive nuclei as well as extracellular citr. H3/MPO-positive foci were assessed.

Induction of NETosis with platelet-rich plasma

Neutrophils from a healthy donor were isolated using a Ficoll-Paque gradient (GE Healthcare) according to manufacturer's instructions and seeded onto Ibidi® μ -Slides (VI 0.4) coated with poly-L lysine (Sigma) by brief centrifugation (40G, 5 min). Platelet-rich plasma (PRP) from 3 CoV_{se} patients and 5 healthy donors was isolated as described previously²², stimulated with 2.3 mM calcium chloride and 20 μ M ADP and subsequently added to the seeded neutrophils for 20 min (37°C, 5% CO₂). Neutrophil-platelet aggregates were fixed with 1% PFA (10 min), permeabilized using 0.5% triton X-100 (10 min) and stained with anti-MPO, anti-citr. H3, anti-CD41 antibodies (HIP8 clone, Biolegend) and Hoechst dye to counterstain nuclei. NETosis and neutrophil-platelet interaction were visualized by immunofluorescence microscopy (six fields of view at 40x magnification per replicate). NETosis was defined according to the criteria mentioned above (see Methods Histopathology).

Neutrophil activation assay by flow cytometry

50 μ l of whole blood from CoV_{se} (n = 3) and healthy controls (n = 5) were incubated with 2.3 mM calcium chloride and 50 nM phorbol myristate acetate (PMA) or DMSO (Ctrl), for 20 min at RT. Treated samples and an untreated control sample were incubated with an antibody panel

for neutrophil activation (CD11b, CD62L, CD63, CD15, *Biologend*) for 10 min, lysed and fixed with 400 FACS Lysing buffer and subsequently analyzed by flow cytometry (BD LSRFortessa Flow Cytometer, data analysis with FlowJo v. 10.6.1, BD).

Platelet and coagulation testing

Platelet and coagulation testing were performed in a subset of included patients. We used the Platelet Function Analyzer (INNOVANCE PFA 200 System, Siemens Healthineers) to assess platelet function under high shear conditions, mimicking primary hemostasis in the arterial system. Briefly, blood was flown through a cartridge containing a membrane either coated with collagen/epinephrine (PFA-EPI) or collagen/ADP (PFA-ADP). Platelet clotting was quantified by measuring closure times by standardized whole blood impedance blood aggregometry (Multiplate Analyzer, Roche Diagnostics) to assess platelet function in Hirudin-anticoagulated blood, excluding a contribution of fibrin formation in this setup. Briefly, changes in impedance after addition of platelet agonists ADP and Thrombin Receptor Activating Peptide (TRAP) were used to assess platelet aggregation over time, readout is standardized by assessing Area under the curve (AUC). In addition to standard INR and aPTT measurements, we performed enhanced analysis of platelet-coagulation interplay and clot-formation under low-shear condition using rotational thrombelastometry (ROTEM, Tem Innovations). This viscoelastic method allows the quantification of the dynamics and thrombus properties during clot-formation and lysis. Briefly, citrate-anticoagulated blood was recalcified and clot formation was initialized by adding start substances activating the intrinsic system (INTEM) or the extrinsic system (EXTEM). A possible effect of heparin was excluded by repeating the INTEM in the presence of Heparinase (HEPTEM). To exclude platelet contribution to clotting, actin-inhibitor Cytochalasin D was added to assess the soluble coagulation cascade in an isolated manner (FIBTEM).

All materials used were obtained from the manufacturer, and all the platelet/coagulation function testing was performed according to published standard protocol in an accredited laboratory setting according to DIN EN ISO 15189.

Data analysis and statistics

Data was analyzed using Excel v.16 (Microsoft) and Prism v. 8.3.0. (GraphPad) software. 3D reconstructions of z-stack data were performed using Imaris (Bitplane). The principal component analysis and heatmaps were created using ClustVis (Flow cytometric analysis for details). Adobe Illustrator was used to assemble the graphical illustrations. Results are shown as mean \pm s.e.m., unless otherwise indicated. For direct comparisons between two groups, unpaired, two-tailed Student's t-tests were used, or in case of platelet and IL-6 time-courses paired t-tests. For comparisons between groups either non-parametric Kruskal-Wallis-tests or two-way ANOVAs were used. A post-hoc Dunn's or Dunnett's multiple comparisons test to the control column (Ctrl) was used. For clarity, only post-hoc test results are displayed in the graphs. If the Kruskal-Wallis or ANOVA test showed a difference between groups without a significant post-hoc test, a bar over the graph indicates the ANOVA/Kruskal-Wallis p value. P values of ≤ 0.05 are considered significant and denoted with *, ≤ 0.01 with ** and ≤ 0.001 with ***. Individual patients are represented as dots, unless otherwise indicated. Reference ranges for laboratory values as used at the patient's hospital, if available, are shown as gray boxes. If there were different reference ranges for male and female patients, the mean of the two was taken as the reference range. For all regression analyses, black lines represent best-fit line, gray area the 95% confidence interval. r^2 and p value (slope non-zero) are shown in plots.

Results & Discussion

We sought to explore tissue injury in COVID-19 by studying histopathological autopsy specimens from a deceased patient with RT-PCR-confirmed SARS-CoV-2 infection and typical findings of COVID-19 pneumonia on CT scans. The patient developed progressive respiratory failure (Horowitz Index, $\text{paO}_2/\text{FiO}_2$ at admission: 457; 6 days later: 132, ref. range > 300), signs of cardiac injury without ECG evidence for macrovascular thrombosis (high-sensitive troponin T concentration 0.798 pg/ml, ref. range < 0.014 ng/ml), kidney failure (glomerular filtration rate 43 ml/min, GFR decrease from admission: 27%) and dysregulated coagulation (D-dimer 3.9 $\mu\text{g/ml}$, ref. range < 0.5 $\mu\text{g/ml}$) over the course of the disease (Fig. 1a-b). Hematoxylin-Eosin staining revealed the formation of microvascular clots in the lung in the absence of pulmonary embolism, similar to observations in lung samples of patients suffering from SARS-CoV-1 infection during the SARS epidemic 2003 (Fig. 1c-d)²³. In addition to platelets and fibrin (Fig. 1d), these thrombi contained large numbers of granulocytes (Fig. 1c inset).

We and others have shown that under certain inflammatory conditions, platelets, neutrophils (abbreviated as PMN) and the coagulation cascade team up to contain invading pathogens, a process termed immunothrombosis^{16, 24}, that can aggravate tissue damage by triggering vessel occlusion and hypoxia²⁵.

To further explore the contribution of immunothrombosis to the pathogenesis of COVID-19, we used immunofluorescence to define the cellular and molecular composition of the microthrombi. We confirmed the presence of neutrophils in the microthrombi, embedded in the fibrin clot (Fig. 1e). We verified this finding in an additional four COVID-19 cases. Here, we observed strongly increased numbers of granulocyte-containing thrombi in COVID-19 autopsies, when compared to lungs from patients deceased due to non-pulmonary pathology (see Fig. 1f


and Fig. IIa in the Supplement). Confocal microscopy revealed numerous intravascular neutrophils in close association with platelets and fibrin (Fig. 1g). Interestingly, these neutrophil-enriched depositions were not restricted to the lung but were also present in renal and cardiac microvessels (Fig. 1g). This led us to hypothesize that dysregulated immunothrombosis driven by activated neutrophils and immunogenic platelets might contribute to organ injury and a systemic thrombogenic state in COVID-19.

We therefore assessed neutrophil dynamics and activation state in two hospitalized COVID-19 cohorts of defined disease severity: (1) severe cases requiring intubation and intensive care treatment (CoV_sev, n=19), and (2) a group of intermediate severity (CoV_int, n=20), which either required no oxygen or received non-invasive supplemental oxygen (Fig. Ia-b in the Supplement). Severe cases showed higher peripheral neutrophil counts, correlating with the degree of lung injury as assessed by the Horowitz Index (Fig. 2a-b).

To gain insight into neutrophil activation patterns in COVID-19, we used a comprehensive high-dimensional flow cytometric activation marker analysis and subsequent t-SNE dimension reduction. Comparing non-COVID-19 pneumonia (Ctrl_pneu) and patients without signs of infection (Ctrl) with CoV_int and CoV_sev cases, we identified distinct activation states (Fig. 2c-d, Table II in the Supplement, Fig. IIb-e in the Supplement and Methods). To characterize the markers responsible for the COVID-19 neutrophil phenotypes, we employed unsupervised clustering and subsequent gating of six neutrophil polarization states (PMN1-PMN6, Fig. 2e-f and Fig. IIIa-c in the Supplement). Interestingly, we found PMN3 sub-cluster to be significantly enhanced in CoV_int cases. This sub-cluster showed a decrease in naïve-neutrophil marker L-selectin (CD62L), and adhesion receptors CD11b and CD49d^{26,27}. Also, FcγRIII (CD16) expression, which negatively correlates with neutrophil apoptosis, was found to be

downregulated (Fig. 2f and Fig. IIIId in the Supplement)²⁷. Therefore, the PMN3 profile points to hyporeactive and apoptotic neutrophils in the circulation of CoV_int patients, possibly reflecting the outcome of neutrophil recruitment and activation in the lung vasculature. In contrast, activation marker CD177 was globally upregulated in severe COVID-19 cases (Fig. IIIId in the Supplement), and the highly activated subpopulation PMN6 was overrepresented in CoV_sev (32.1 ±12.9% of neutrophils in CoV_sev, vs. 8.8 ±3.3% in controls, Fig. 2f). CD177 furthermore correlated significantly with pulmonary disease severity, underlining a potentially causative role of neutrophils (Fig. 2g). Isolation and staining of peripheral blood neutrophils from CoV_sev patients showed increased activation of these cells in the circulation compared to controls (Fig. 2h). In line, *in vitro* stimulation of CoV_sev neutrophils with phorbol myristate acetate (PMA) revealed a differential response with increased CD63 expression indicating granule release, and decreased expression of adhesion receptor CD11b in COVID-19 compared to controls (Fig. IIIe in the Supplement). In summary, distinct neutrophil signatures exist in different courses of COVID-19 ranging from a hyporeactive phenotype in intermediate COVID-19 patients to an excessive, global neutrophil activation characterizing severe COVID-19. Platelets are major initiators of neutrophil activation and boost neutrophil-driven tissue damage²². Indeed, in COVID-19 patients formation of circulating platelet-neutrophil-aggregates, a key element of immunothrombosis²⁴, correlated in a linear fashion with pulmonary disease severity (Fig. 2i).

Given the central role of platelets driving immunothrombosis^{22, 28}, we analyzed quantitative and qualitative changes of platelets. In COVID-19, thrombocytopenia at hospital admission is reported in more severe cases, hinting at platelet consumption²⁹. In line with this notion, platelet counts in our cohort of COVID-19 patients were at the lower end of the normal range (Fig. 3a, Fig. IVa in the Supplement). A longitudinal assessment of platelet counts

revealed highly dynamic changes over time, particularly in patients admitted to ICU and requiring intubation (Fig. 3b). When assessing individual platelet levels, 81% of COVID-19 patients showed an increase (50% or more) during hospital stay (21/26 patients, Fig. 3c), and 50% of patients even developed mild thrombocytosis (platelet count $>360.000/\mu\text{l}$, 13/26 patients). Interleukin-6 (IL-6) has been causally linked to TPO transcription and increased thrombopoiesis³⁰. We correlated IL-6 plasma levels and platelet counts in CoV_sev and CoV_int patients (Fig. 3b). In severe cases, IL-6 peaked at the time of intubation/ICU admission and was followed by a peak in platelet count with a lag of five days (Fig. 3b-c). We observed a similar trend in the intermediate cohort (Fig. IVb in the Supplement), indicating a link between the acute phase inflammatory response and a reactive increase in platelet production in COVID-19³¹⁻³³. Hematocrit levels of CoV_int and CoV_sev patients decreased over the disease course,  excluding dehydration as the reason for increased platelet count (Fig. IVc in the Supplement).

To assess whether this quantitative shift in the platelet compartment was accompanied by phenotypic changes, we employed comprehensive antibody-based surface marker analysis (Fig. Va-b in the Supplement, Table III in the Supplement, Methods). We performed t-SNE based unsupervised clustering, which uncovered distinct changes in platelet marker profiles in intermediate and severe COVID-19 cases, compared to both non-COVID-19 pneumonia patients and patients without signs of infection (Fig. 3d-e and Fig. Vb in the Supplement). We confirmed this finding using Principal Component Analysis, which revealed distinct platelet activation patterns with a strong correlation to disease severity (Fig. Vc-d in the Supplement). To gain insight into these distinct marker profiles, we performed clustering of platelet populations in a robust manner (unsupervised clustering with Phenograph followed by subsequent supervised gating), defining 10 sub-clusters (Plt1-10)³⁴ (Fig. 3f and Fig. VIa-b in the Supplement). Two out

of 10 identified sub-clusters were significantly enriched in CoV_int (Plt9 and Plt10), and one out of 10 populations was enriched in CoV_sev (Plt4) (Fig. 3g, Fig. VIb-c in the Supplement). All COVID-19 enriched clusters as well as global expression analysis (Fig. VI d in the Supplement) showed downregulation of scavenger receptor CD36 and transmembrane protein CD40L in comparison to control patients.

In CoV_int patients, an expression heatmap revealed generalized downregulation of platelet adhesion receptors, including CD41, CD31 and PSGL-1. In addition, Toll-like receptor 4 (TLR-4) and C-X-C Motif Chemokine Receptor 4 (CXCR4), which have been implicated in platelet host defense²⁵, were decreased. Compared to control cohorts, markers of platelet activation such as CD63, activated integrin GPIIbIIIa (PAC-1) and CD62P were downregulated or detected at similar levels in CoV_int (Fig. VI d in the Supplement).

In contrast, we identified a small but highly activated platelet population in some CoV_sev patients (Plt1, 10.0% \pm 4.5 of platelets in CoV_sev, vs. 3.1% \pm 0.7 in controls, Fig. 3g). Plt4 subcluster, which was enriched in CoV_sev, showed low expression of GpIIbIIIa and CD36, comparable to CoV_int clusters, but exhibited a higher level of activation of immune receptors like CLEC-2 (Fig. 3g), which also applied to the composite platelet heatmap (Fig. Vd in the Supplement).

The overall hyporeactive phenotype in peripheral blood, in combination with evidence of recruitment to the pulmonary, renal, and cardiac microvasculature, suggested platelet activation within the microvasculature and subsequent circulation of exhausted platelets, in line with our data on neutrophils. Indeed, after activation and sequestration in the lung, exhausted platelets have been shown to recirculate in blood^{35, 36}. Along these lines, lower CD40L densities known to



mediate platelet-leukocyte interaction as well as decreased scavenger receptor CD36 densities can be explained by activation and receptor shedding in the pulmonary vasculature^{37, 38}.

As these data suggest a profound impact of COVID-19 on peripheral platelet function, we next assessed primary hemostasis under high shear conditions using the PFA-200 system (Fig. 3h, see Methods). CoV_int patients showed normal response to Collagen-Epinephrine as well as Collagen-ADP matrices. In CoV_sev, we found increased plug formation in both tests compared to CoV_int (Fig. 3h). This might be caused by the aforementioned highly activated Plt1 subpopulation present in CoV_sev patients.

Whole-blood impedance aggregometry showed mild reduction in platelet aggregation in COVID-19, with 41% of patients (7/17) below reference range following adenosine diphosphate (ADP) stimulation (Fig. 3i). This finding was mainly driven by hyporeactivity of CoV_int cases in response to ADP and thrombin-receptor agonist TRAP, with a less pronounced effect in CoV_sev. In a separate experiment, we measured platelet activation upon stimulation with various agonists, which confirmed a dysregulated platelet phenotype in severe COVID-19, showing hyperreactivity towards weak agonists with a decreased maximal response towards strong agonists (see Fig. VIe in the Supplement). In conclusion, platelet function analysis uncovered normal to (mildly) reduced platelet responses in CoV_int cases, in accordance with the hyporeactive platelet phenotype revealed by expression analysis. In CoV_sev patients, we revealed a more complex activation pattern with signs of thrombogenic hyperreactivity and immunologic exhaustion.

Next, we defined whether changes in neutrophil and platelet activation are associated with changes in systemic plasmatic coagulation parameters in COVID-19 patients. In our cohort, INR and aPTT values were found to be within physiological range (Fig. 4a). As previously

published, intermediate and severe COVID-19 patients exhibited elevated plasma fibrinogen, with almost 90% above reference range (27/31 patients, Fig. 4b)¹⁴. Interestingly, fibrinogen levels correlated significantly with Horowitz Index ($\text{paO}_2/\text{FiO}_2$), a surrogate parameter for classification of ARDS severity (Fig. 4c). Ferritin, another acute phase protein previously described to be associated with COVID-19 severity, correlated to lesser extent (Fig. VIIa in the Supplement). This could hint at a specific effect of SARS-CoV-2 on fibrinogen plasma levels beyond the canonical acute phase response. Along these lines, the related strain SARS-CoV-1, the causative coronavirus in the 2003 SARS outbreak, was reported to directly upregulate fibrinogen expression in infected cells³⁹.

We also found fibrin degradation product D-Dimer to be strongly elevated in COVID-19 (mean 1.93 $\mu\text{g/ml}$), with 65% (13/20 patients) of CoV_int and all (11/11 patients) CoV_sev patients above reference range (Fig. 4d), pointing to constant activation of the coagulation cascade in COVID-19 patients. In addition, D-Dimer also correlated significantly with disease severity (Fig. VIIb in the Supplement).

Two important causes of elevated D-Dimer are disseminated intravascular coagulation (DIC) and macrovascular thrombosis, both complications of COVID-19^{15, 40}. However, normal to elevated platelet counts and elevated fibrinogen, in combination with normal aPTT and INR, excluded DIC in our cohort. All CoV_sev patients received prophylactic heparin treatment, and no event of macrovascular thrombosis (defined as stroke, myocardial infarction, or venous thromboembolism) was diagnosed at the time of enrollment in this closely monitored ICU cohort^{15, 41}, suggesting microvascular (immuno)thrombosis as the possible culprit.

To more specifically assess platelet-coagulation interplay and clot-formation under low-shear conditions, we employed rotational thrombelastometry (ROTEM). Intrinsic (INTEM) and extrinsic (EXTEM) activation of clot formation revealed clot formation times (CFT), maximal clot firmness (MCF) and clotting times (CT) within the reference range for non-severe CoV_int cases (Fig. 4e-f, Fig. VIIc in the Supplement). Addition of heparinase (HEPTTEM) to exclude a possible heparin-mediated effect showed similar MCF and CFT results (Fig. VIId in the Supplement). However, in CoV_sev patients, MCF was significantly increased, and CFT shortened compared to CoV_int (Fig. 4e and 4f). INTEM and EXTEM clot formation correlated with neutrophil counts as well as disease severity, exhibiting decreased clot formation time and increased clot firmness in more severe cases (Fig. 4g and Fig. VIIe-g in the Supplement). Clotting time (CT) was within reference range and did not differ between CoV_int and CoV_sev, indicating that clotting factors are not the main drivers of the differences in MCF and CFT (Fig. VIIc in the Supplement). Following clot formation, maximum lysis (ML) of clots was also reduced in CoV_sev, and clot resistance to lysis correlated strongly with disease severity (Fig. 4h-i).

Lastly, we excluded platelet contribution to clot formation by addition of actin polymerization inhibitor Cytochalasin D. This revealed platelet independent heightened plasmonic clot formation (FIBTEM) in severe and intermediate cases, with 53% above reference range for maximal clot firmness (MCF, 9/17 patients, Fig. 4j). We hypothesized that increased clot formation might be, in part, caused by the considerably elevated fibrinogen plasma concentrations in COVID-19. Indeed, plasma concentrations of fibrinogen and FIBTEM MCF correlated strongly in our cohort (Fig. 4k), providing indirect evidence to this concept.

In summary, plasmatic coagulation is skewed towards a procoagulant state correlating with disease severity, reflected by peripheral blood coagulation tests as well as histopathological evidence of microvascular thrombosis in affected organs.

Mechanistically, we uncovered dynamic quantitative and qualitative changes in neutrophil and platelet compartments in COVID-19, in addition to histopathological and flow cytometric evidence of a partnership between these two cell types. Platelets are known to regulate neutrophil recruitment⁴². In particular, activated platelets have been shown to be critically involved in neutrophil extracellular trap (NET) formation, a central element of immunothrombosis^{24, 43, 44}. NETs have high procoagulant potential, and could therefore serve as a link to explain altered blood coagulation and microvascular thrombosis in SARS-CoV-2 infection⁴⁵. Indeed, elevated markers of NETosis have been found in COVID-19, correlating with disease severity⁴⁶.

To underline our hypothesis that partnership of neutrophils and dysregulated platelets drives NET formation and thereby possibly immunothrombosis in COVID-19, we superfused neutrophils isolated from healthy donors with activated platelet rich plasma from either CoV_sev or control patients (Fig. 4l). Platelets from severe COVID-19 patients showed increased adhesion to neutrophils (Fig. 4m, Fig. VIIh in the Supplement), and resulted in enhanced NET formation, underlining the mechanistic link of immunogenic platelets driving neutrophil activation in COVID-19 (Fig. 4n, Fig. VIIi in the Supplement).

Finally, we re-analyzed tissue sections for the presence of microvascular NETs. Indeed, we discovered frequent intravascular NETs derived from neutrophils in the pulmonary vasculature, which were found to be virtually absent in control lungs (Fig. 4o and p). Interestingly, NET-like structures were not only found in the pulmonary vasculature, but also in

kidney and heart specimens (Fig 4q and r). These structures were also spatially associated with fibrin deposition, underlining their procoagulant role (Fig. 4o and p).

Taken together, we provide evidence that platelets, neutrophils, and the coagulation cascade are drivers of disease severity and might prove to be valuable pharmacological targets in COVID-19 (Fig. VIII in the Supplement, Graphical abstract). In addition, SARS-CoV-2 infected patients are at risk for increased thrombotic events, making prophylactic anticoagulation and vigilant monitoring for thrombotic complications a central task in management of COVID-19 patients.

Acknowledgments

The authors thank the patients and their families for donating their blood and for their participation in the CORKUM registry. We thank Kornelia Lesser-Wetzold for her technical assistance, and Anna Titova for her help with histology. We would like to thank all CORKUM investigators and staff.



Authorship contributions

Initiation, L.N., A.L.; Conceptualization, L.N., K.P., and K.S.; Methodology, L.N., K.P., A.L., S.B., M.R., Investigation, L.N., K.P., A.L, S.B., R.K., T.W., M.W., B.Z., M.R., S.L, H.S., M.M.; Resources, S.M., J.H, C.S., K.S., D.T. O.K., M.B-B., S.K.; Formal Analysis, L.N., K.P., A.L., S.B., R.K.; Writing – Original Draft, L.N.; Writing – Editing, all authors; Visualization, L.N., K.P. and A.L.; Supervision, L.N., K.P., K.S.; Project Administration, L.N., K.P and K.S.; Funding Acquisition, L.N., K.P., S.M. and K.S.

Sources of Funding: This study was supported by the Deutsche Forschungsgemeinschaft (DFG) SFB 914 (S.M. [B02 and Z01], K.S. [B02]), the DFG SFB 1123 (S.M. [B06], K.S. [A07]), the DFG FOR 2033 (S.M.), the German Centre for Cardiovascular Research (DZHK) (Clinician Scientist Programme [L.N.], MHA 1.4VD [S.M.]), FP7 program (project 260309, PRESTIGE [S.M.]), FöFoLe project 1015/1009 (L.N.), and the DFG Clinician Scientist Programme PRIME (413635475, K.P., R.K.) . The work was also supported by the European Research Council (ERC-2018-ADG "IMMUNOTHROMBOSIS" [S.M.]).

Disclosures

The authors declare no conflict of interest.



Supplemental Materials

Supplemental Figures I-VIII

Supplemental Tables I-III

Authors

Leo Nicolai, MD^{1,2,#,*}; Alexander Leunig, BA^{1,2,#}; Sophia Brambs, cand med¹;
 Rainer Kaiser, MD^{1,2}; Tobias Weinberger, MD^{1,2}; Michael Weigand, MD³;
 Maximilian Muenchhoff, MD^{4,5}; Johannes C. Hellmuth, MD^{6,7}; Stephan Ledderose, MD⁸;
 Heiko Schulz, MD⁸; Clemens Scherer, MD^{1,2}; Martina Rudelius, MD⁸; Michael Zoller, MD⁹;
 Dominik Höchter, MD⁹; Oliver Keppler, MD^{4,5}; Daniel Teupser, MD³; Bernhard Zwißler, MD⁹;
 Michael von Bergwelt-Baildon, MD^{6,7}; Stefan Kääb, MD^{1,2}; Steffen Massberg, MD^{1,2};
 Kami Pekayvaz, MD^{1,2,§,*}; Konstantin Stark, MD^{1,2,§}

¹Medizinische Klinik und Poliklinik I, University Hospital Ludwig-Maximilian-University Munich, Munich, Germany; ²DZHK (German Centre for Cardiovascular Research), partner site Munich Heart Alliance, 80802 Munich, Germany; ³Institute of Laboratory Medicine, University Hospital Ludwig-Maximilian-University Munich, Munich, Germany; ⁴Virology, Max von Pettenkofer Institute, Ludwig-Maximilian-University Munich, Munich, Germany; ⁵German Center for Infection Research (DZIF), Partner Site Munich, Munich, Germany; ⁶Medizinische Klinik und Poliklinik III, University Hospital Ludwig-Maximilian-University Munich, Munich, Germany; ⁷German Cancer Consortium (DKTK), Munich, Bavaria 81377, Germany; ⁸Institute of Pathology, Ludwig-Maximilian-University, Munich, Germany; ⁹Department of Anesthesiology, University Hospital Ludwig-Maximilian-University Munich, Munich, Germany

contributed equally

§ contributed equally

*Co-corresponding authors



Circulation

References

1. Zhu N, Zhang D, Wang W, Li X, Yang B, Song J, Zhao X, Huang B, Shi W and Lu R. A novel coronavirus from patients with pneumonia in China, 2019. *New England Journal of Medicine*. 2020:727-733.
2. Zhou P, Yang X-L, Wang X-G, Hu B, Zhang L, Zhang W, Si H-R, Zhu Y, Li B, Huang C-L, Chen H-D, Chen J, Luo Y, Guo H, Jiang R-D, Liu M-Q, Chen Y, Shen X-R, Wang X, Zheng X-S, Zhao K, Chen Q-J, Deng F, Liu L-L, Yan B, Zhan F-X, Wang Y-Y, Xiao G-F and Shi Z-L. A pneumonia outbreak associated with a new coronavirus of probable bat origin. *Nature*. 2020;579:270-273.
3. Ruan Q, Yang K, Wang W, Jiang L and Song J. Clinical predictors of mortality due to COVID-19 based on an analysis of data of 150 patients from Wuhan, China. *Intensive care medicine*. 2020:846-848.
4. Wu Z and McGoogan JM. Characteristics of and important lessons from the coronavirus disease 2019 (COVID-19) outbreak in China: summary of a report of 72 314 cases from the Chinese Center for Disease Control and Prevention. *Jama*. 2020:1239-1242.

5. Cao B, Wang Y, Wen D, Liu W, Wang J, Fan G, Ruan L, Song B, Cai Y and Wei M. A trial of lopinavir–ritonavir in adults hospitalized with severe Covid-19. *New England Journal of Medicine*. 2020:1787-1799.
6. Guan W-j, Ni Z-y, Hu Y, Liang W-h, Ou C-q, He J-x, Liu L, Shan H, Lei C-l and Hui DSC. Clinical characteristics of coronavirus disease 2019 in China. *New England Journal of Medicine*. 2020:1708-1720.
7. Zhou F, Yu T, Du R, Fan G, Liu Y, Liu Z, Xiang J, Wang Y, Song B and Gu X. Clinical course and risk factors for mortality of adult inpatients with COVID-19 in Wuhan, China: a retrospective cohort study. *The Lancet*. 2020;395:1054-1062.
8. Cheng Y, Luo R, Wang K, Zhang M, Wang Z, Dong L, Li J, Yao Y, Ge S and Xu G. Kidney disease is associated with in-hospital death of patients with COVID-19. *Kidney international*. 2020;97:829-83.
9. Guo T, Fan Y, Chen M, Wu X, Zhang L, He T, Wang H, Wan J, Wang X and Lu Z. Cardiovascular Implications of Fatal Outcomes of Patients With Coronavirus Disease 2019 (COVID-19). *JAMA Cardiology*. 2020:811-818.
10. Shi S, Qin M, Shen B, Cai Y, Liu T, Yang F, Gong W, Liu X, Liang J, Zhao Q, Huang H, Yang B and Huang C. Association of Cardiac Injury With Mortality in Hospitalized Patients With COVID-19 in Wuhan, China. *JAMA Cardiology*. 2020:802-810.
11. Xu Z, Shi L, Wang Y, Zhang J, Huang L, Zhang C, Liu S, Zhao P, Liu H and Zhu L. Pathological findings of COVID-19 associated with acute respiratory distress syndrome. *The Lancet respiratory medicine*. 2020;8:420-422.
12. Wang T, Chen R, Liu C, Liang W, Guan W, Tang R, Tang C, Zhang N, Zhong N and Li S. Attention should be paid to venous thromboembolism prophylaxis in the management of COVID-19. *The Lancet Haematology*. 2020:362-363.
13. Tang N, Bai H, Chen X, Gong J, Li D and Sun Z. Anticoagulant treatment is associated with decreased mortality in severe coronavirus disease 2019 patients with coagulopathy. *Journal of thrombosis and haemostasis*. 2020;18:1094-1099.
14. Han H, Yang L, Liu R, Liu F, Wu KL, Li J, Liu XH and Zhu CL. Prominent changes in blood coagulation of patients with SARS-CoV-2 infection. *Clinical chemistry and laboratory medicine*. 2020:1116-1120.
15. Cui S, Chen S, Li X, Liu S and Wang F. Prevalence of venous thromboembolism in patients with severe novel coronavirus pneumonia. *Journal of Thrombosis and Haemostasis*. 2020;18:1421-1424.
16. Massberg S, Grahl L, von Bruehl ML, Manukyan D, Pfeiler S, Goosmann C, Brinkmann V, Lorenz M, Bidzhekov K, Khandagale AB, Konrad I, Kennerknecht E, Reges K, Holdenrieder S, Braun S, Reinhardt C, Spannagl M, Preissner KT and Engelmann B. Reciprocal coupling of coagulation and innate immunity via neutrophil serine proteases. *Nature medicine*. 2010;16:887-96.
17. Engelmann B and Massberg S. Thrombosis as an intravascular effector of innate immunity. *Nature reviews Immunology*. 2013;13:34-45.
18. Simon M, Wachs C, Braune S, de Heer G, Frings D and Kluge S. High-Flow Nasal Cannula Versus Bag-Valve-Mask for Preoxygenation Before Intubation in Subjects With Hypoxemic Respiratory Failure. *Respiratory care*. 2016;61:1160-7.
19. Marx C, Novotny J, Salbeck D, Zellner KR, Nicolai L, Pekayvaz K, Kilani B, Stockhausen S, Bürgener N, Kupka D, Stocker TJ, Weckbach LT, Pircher J, Moser M, Joner M, Desmet W, Adriaenssens T, Neumann F-J, Gerschlick AH, Ten Berg JM, Lorenz M and Stark K.

- Eosinophil-platelet interactions promote atherosclerosis and stabilize thrombosis with eosinophil extracellular traps. *Blood*. 2019;134:1859-1872.
20. Levine JH, Simonds EF, Bendall SC, Davis KL, Amir E-aD, Tadmor MD, Litvin O, Fienberg HG, Jager A, Zunder ER, Finck R, Gedman AL, Radtke I, Downing JR, Pe'er D and Nolan GP. Data-Driven Phenotypic Dissection of AML Reveals Progenitor-like Cells that Correlate with Prognosis. *Cell*. 2015;162:184-197.
 21. Metsalu T and Vilo J. ClustVis: a web tool for visualizing clustering of multivariate data using Principal Component Analysis and heatmap. *Nucleic acids research*. 2015;43:W566-70.
 22. Gaertner F, Ahmad Z, Rosenberger G, Fan S, Nicolai L, Busch B, Yavuz G, Luckner M, Ishikawa-Ankerhold H and Hennel R. Migrating platelets are mechano-scavengers that collect and bundle bacteria. *Cell*. 2017;171:1368-1382. e23.
 23. Ding Y, Wang H, Shen H, Li Z, Geng J, Han H, Cai J, Li X, Kang W and Weng D. The clinical pathology of severe acute respiratory syndrome (SARS): a report from China. *The Journal of Pathology: A Journal of the Pathological Society of Great Britain and Ireland*. 2003;200:282-289.
 24. Clark SR, Ma AC, Tavener SA, McDonald B, Goodarzi Z, Kelly MM, Patel KD, Chakrabarti S, McAvoy E, Sinclair GD, Keys EM, Allen-Vercoe E, Devinney R, Doig CJ, Green FH and Kubes P. Platelet TLR4 activates neutrophil extracellular traps to ensnare bacteria in septic blood. *Nature medicine*. 2007;13:463-9.
 25. Nicolai L, Gaertner F and Massberg S. Platelets in Host Defense: Experimental and Clinical Insights. *Trends in Immunology*. 2019;40:922-938.
 26. Silvestre-Roig C, Hidalgo A and Soehnlein O. Neutrophil heterogeneity: implications for homeostasis and pathogenesis. *Blood, The Journal of the American Society of Hematology*. 2016;127:2173-2181.
 27. Dransfield I, Buckle AM, Savill JS, McDowall A, Haslett C and Hogg N. Neutrophil apoptosis is associated with a reduction in CD16 (Fc gamma RIII) expression. *The Journal of Immunology*. 1994;153:1254-1263.
 28. Gaertner F and Massberg S. Patrolling the vascular borders: platelets in immunity to infection and cancer. *Nature Reviews Immunology*. 2019:747-760.
 29. Lippi G, Plebani M and Henry BM. Thrombocytopenia is associated with severe coronavirus disease 2019 (COVID-19) infections: A meta-analysis. *Clinica Chimica Acta*. 2020;506:145-148.
 30. Kaser A, Brandacher G, Steurer W, Kaser S, Offner FA, Zoller H, Theurl I, Widder W, Molnar C, Ludwiczek O, Atkins MB, Mier JW and Tilg H. Interleukin-6 stimulates thrombopoiesis through thrombopoietin: role in inflammatory thrombocytosis. *Blood*. 2001;98:2720-5.
 31. Ishiguro A, Suzuki Y, Mito M, Shimbo T, Matsubara K, Kato T and Miyazaki H. Elevation of serum thrombopoietin precedes thrombocytosis in acute infections. *Br J Haematol*. 2002;116:612-8.
 32. Schafer AI. Thrombocytosis. *New England Journal of Medicine*. 2004;350:1211-1219.
 33. Prina E, Ferrer M, Ranzani OT, Polverino E, Cillóniz C, Moreno E, Mensa J, Montull B, Menéndez R, Cosentini R and Torres A. Thrombocytosis Is a Marker of Poor Outcome in Community-Acquired Pneumonia. *Chest*. 2013;143:767-775.
 34. Reyes M, Filbin MR, Bhattacharyya RP, Billman K, Eisenhaure T, Hung DT, Levy BD, Baron RM, Blainey PC, Goldberg MB and Hacohen N. An immune-cell signature of bacterial sepsis. *Nature medicine*. 2020;26:333-340.

35. Cloutier N, Allaeyes I, Marcoux G, Machlus KR, Mailhot B, Zufferey A, Levesque T, Becker Y, Tessandier N, Melki I, Zhi H, Poirier G, Rondina MT, Italiano JE, Flamand L, McKenzie SE, Cote F, Nieswandt B, Khan WI, Flick MJ, Newman PJ, Lacroix S, Fortin PR and Boilard E. Platelets release pathogenic serotonin and return to circulation after immune complex-mediated sequestration. *Proceedings of the National Academy of Sciences*. 2018;115:E1550.
36. Pareti FI, Capitanio A, Mannucci L, Ponticelli C and Mannucci PM. Acquired dysfunction due to the circulation of “exhausted” platelets. *The American journal of medicine*. 1980;69:235-240.
37. Tariket S, Hamzeh-Cognasse H, Laradi S, Arthaud C-A, Eyraud M-A, Bourlet T, Berthelot P, Garraud O and Cognasse F. Evidence of CD40L/CD40 pathway involvement in experimental transfusion-related acute lung injury. *Scientific Reports*. 2019;9:12536.
38. Werner JL and Steele C. Innate receptors and cellular defense against pulmonary infections. *Journal of immunology (Baltimore, Md : 1950)*. 2014;193:3842-3850.
39. Tan Y-J, Tham P-Y, Chan DZL, Chou C-F, Shen S, Fielding BC, Tan THP, Lim SG and Hong W. The severe acute respiratory syndrome coronavirus 3a protein up-regulates expression of fibrinogen in lung epithelial cells. *Journal of virology*. 2005;79:10083-10087.
40. Tang N, Li D, Wang X and Sun Z. Abnormal coagulation parameters are associated with poor prognosis in patients with novel coronavirus pneumonia. *J Thromb Haemost*. 2020;18:844-847.
41. Klok FA, Kruip MJHA, van der Meer NJM, Arbous MS, Gommers DAMPJ, Kant KM, Kaptein FHJ, van Paassen J, Stals MAM, Huisman MV and Endeman H. Incidence of thrombotic complications in critically ill ICU patients with COVID-19. *Thrombosis research*. 2020:145-147.
42. Sreeramkumar V, Adrover JM, Ballesteros IC, Maria Isabel , Rossaint J, Bilbao I, Nacher MP, Christophe Radovanovic, Irena , Fukui YM, Rodger P. Filippi, Marie-Dominique Lizasoain, Ignacio and Ruiz-Cabello JZ, Alexander Hidalgo, Moro, María A. Andrés Neutrophils scan for activated platelets to initiate inflammation. *Science*. 2014;346:1234-8.
43. Castanheira FVS and Kubes P. Neutrophils and NETs in modulating acute and chronic inflammation. *Blood*. 2019;133:2178-2185.
44. Brinkmann V, Reichard U, Goosmann C, Fauler B, Uhlemann Y, Weiss DS, Weinrauch Y and Zychlinsky A. Neutrophil extracellular traps kill bacteria. *Science*. 2004;303:1532-5.
45. Gould TJ, Vu TT, Swystun LL, Dwivedi DJ, Mai SHC, Weitz JI and Liaw PC. Neutrophil extracellular traps promote thrombin generation through platelet-dependent and platelet-independent mechanisms. *Arteriosclerosis, thrombosis, and vascular biology*. 2014;34:1977-1984.
46. Zuo Y, Yalavarthi S, Shi H, Gockman K, Zuo M, Madison JA, Blair CN, Weber A, Barnes BJ, Egeblad M, Woods RJ, Kanthi Y and Knight JS. Neutrophil extracellular traps in COVID-19. *JCI Insight*. 2020:e138999.

Figure Legends

Figure 1. COVID-19-associated coagulopathy in the lung, kidney and heart presents as

microvascular immunothrombosis. a, COVID-19 disease progression of autopsy case.

Horowitz oxygenation index (paO_2/FiO_2), as well as Interleukin 6 (IL-6), high-sensitive

Troponin T and glomerular filtration rate (GFR) are plotted. **b,** Axial and coronal computed

tomographic (CT) scans of the chest of the patient at presentation with COVID-19 defining

bipulmonary infiltrates and ground glass opacities. **c,** Hematoxylin Eosin (HE) staining of a

pulmonary microthrombus. Immune cells, most notably cells with segmented nuclei, can be

observed in the thrombus (black arrows). **d,** Elastica van Gieson, fibrinogen and platelet

(CD42b) immunohistochemistry of the lung microthrombus. **e,** Exemplary immunofluorescence

of a cut through a lung microthrombus showing of neutrophils (MPO) and fibrinogen. Dashed

lines indicate vessel borders. Scale bars=100 μ m. **f,** Percentage of vessels with

immunothrombosis (platelets, fibrinogen, neutrophils) in the lung vasculature. n=5 controls, n=5

COVID-19 autopsy cases. Two-tailed unpaired t-test. **g,** Immunofluorescence staining of

intravascular microthrombi with spatial association of neutrophils (MPO), platelets (Plt, CD42b)

and fibrin. Scale bars: 10 μ m, dashed lines indicate vessel borders. ** p<0.01.

Figure 2. High dimensional analysis of neutrophil markers reveals a distinct neutrophil

signature, characterized by overshooting, global neutrophil activation in severe disease. a,

Neutrophil count of COVID-19 patients from white blood cell differential. N=19 CoV_int, n=10

CoV_sev, two-tailed unpaired Student's t-test. Reference range for neutrophil counts is shown in

gray (1.85 to 6.8 G/l). **b,** Linear regression of neutrophil count with Horowitz Index (paO_2/FiO_2)

of patients at blood draw. n=19 CoV_int, n=10 CoV_sev. **c-f**, t-Distributed Stochastic Neighbor Embedding (t-SNE) of neutrophil heterogeneity panel of Ctrl, Ctrl_pneu, CoV_int and CoV_sev (n=25,000 down-sampled cells per group). n=7 Ctrl, n=4 Ctrl_pneu, n=11 CoV_int, n=5 CoV_sev patients. **c**, t-SNE plot **d**, t-SNE density plot displaying polarization of each group. **e**, Color-coded phenograph-based sub-clusters of the t-SNE plot are shown. **f**, Heatmap of the mean fluorescence intensity (MFI) for neutrophil sub-clusters relative to the maximum MFI. See Methods for the exact clustering of the heatmap. For PMN 3 and PMN 6 the percentages of total neutrophils of each patient within this sub-cluster are annotated in violin plots. Percentages of neutrophils in each sub-cluster are shown in gray above the heatmap. Kruskal-Wallis test and post-hoc Dunn's multiple comparison test. Line denotes significant Kruskal-Wallis test, but non-significant post-hoc test. **g**, Linear regression of CD177 expression of neutrophils with Horowitz Index. n=10 CoV_int, n=5 CoV_sev. **h**, Percent of activated neutrophils in COVID-19 and control blood assessed by citH3 and MPO membrane blebbing in 6 high-power fields per patient. Representative micrographs are shown on the left. n=5 controls, n=3 CoV_sev. Two-tailed unpaired Student's t-test. **i**, Linear regression of neutrophil platelet aggregates as percentage of total blood leukocytes with Horowitz Index. n=10 CoV_int, n=5 CoV_sev. * p<0.05, ** p<0.01.

Figure 3. High dimensional analysis of platelet markers and platelet function tests reveal a distinct platelet phenotype. a, Platelet count on the day of admission for intermediate (CoV_int n=19) and severe COVID-19 patients (CoV_sev n=7). Reference range for platelet counts is shown in gray (160 to 360 x1000/ μ l). **b**, Time course of platelet count (red spheres) and Interleukin-6 (IL-6) (white triangles) of CoV_sev patients normalized to the day of ICU admission. Number of patients for each time point shown above. Gray: reference range for

platelet counts. **c**, Changes in platelet count and IL-6 measurements over time (days) in CoV_{sev} patients. Gray: reference range for platelet counts (160 to 360 x1000/ μ l). n=8 for PLTC, n=9 for IL-6. Two-tailed paired t-test. **d**, t-Distributed Stochastic Neighbor Embedding (t-SNE) of platelet heterogeneity panel of Ctrl, Ctrl_pneu, CoV_{int} and CoV_{sev} (n=40,000 down-sampled cells per group). **e**, t-SNE plot displayed separately for each group, represented as a density plot. **f**, Color-coded Phenograph platelet subclusters. **g**, Heatmap of the mean fluorescence intensity (MFI) for each platelet subcluster relative to the maximum MFI of the surface marker. See Methods for the exact clustering of the heatmap. For subcluster population Plt 1, 4, 9 and 10, the percentages of total platelets of each patient within this subcluster are annotated in violin plots. Percentages of platelets in each subcluster are shown in gray above the heatmap. Kruskal-Wallis test and a post-hoc Dunn's multiple comparison test. Line denotes significant Kruskal-Wallis test, but non-significant post-hoc test. **d-g**: n=7 Ctrl, n=4 Ctrl_pneu, n=11 CoV_{int}, n=5 CoV_{sev} patients. **h**, Platelet function analyzer-200 (PFA) results for collagen/epinephrine (EPI) and collagen/ADP (ADP). Gray: reference ranges for the PFA test (PFA EPI: 84-160s PFA ADP: 68-121s). n=9 CoV_{int}, n=8 CoV_{sev}, two-tailed unpaired Student's t-test. **i**, Whole blood impedance aggregometry (Multiplate®, MP) results for thrombin-receptor agonist peptide (TRAP) and adenosine diphosphate (ADP) stimulation. Gray: reference ranges for the MP test (MP TRAP: 76-154U, MP ADP: 53-122U). n=9 CoV_{int}, n=8 CoV_{sev}. * p<0.05, ** p<0.01, *** p<0.001.

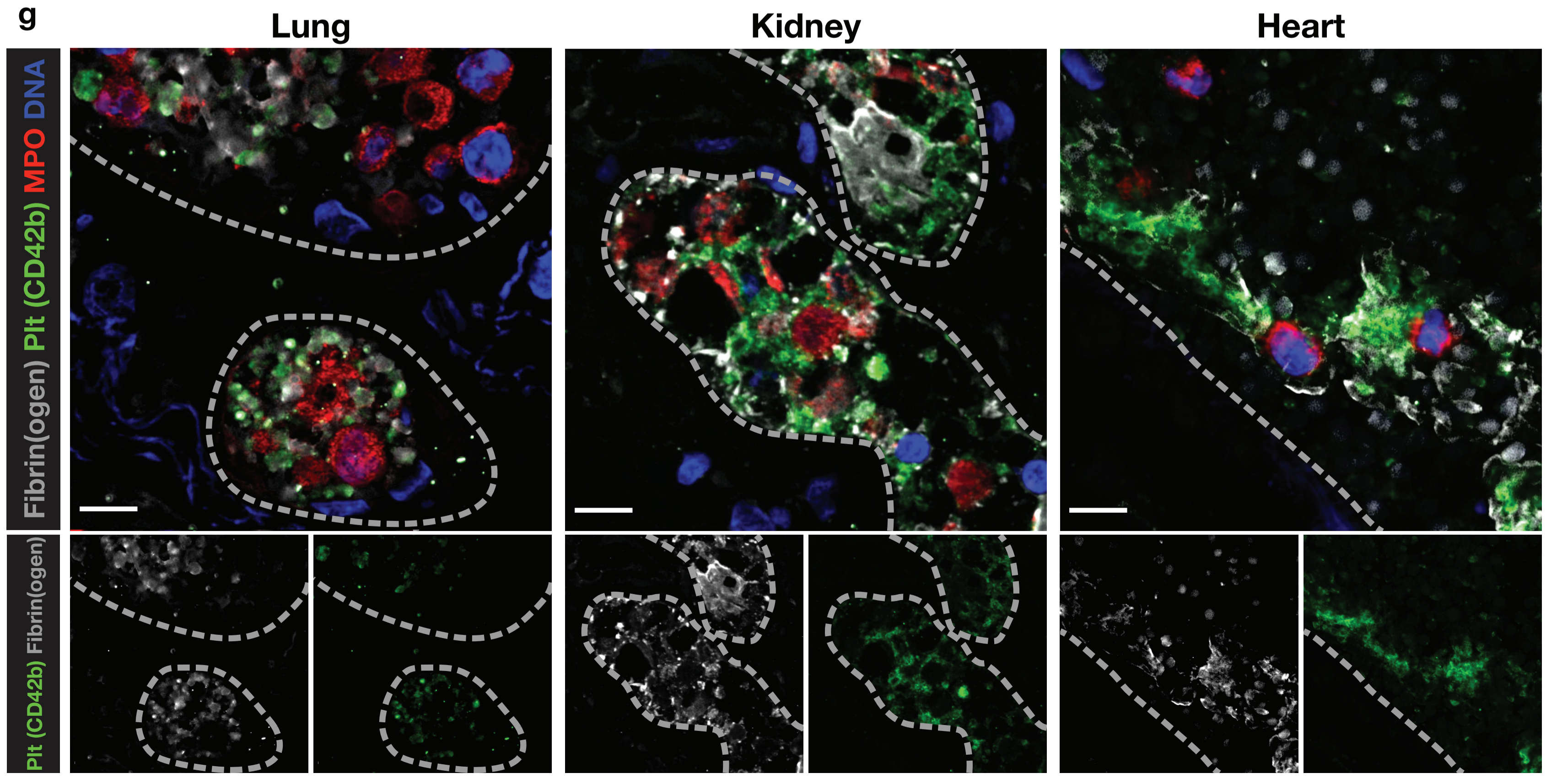
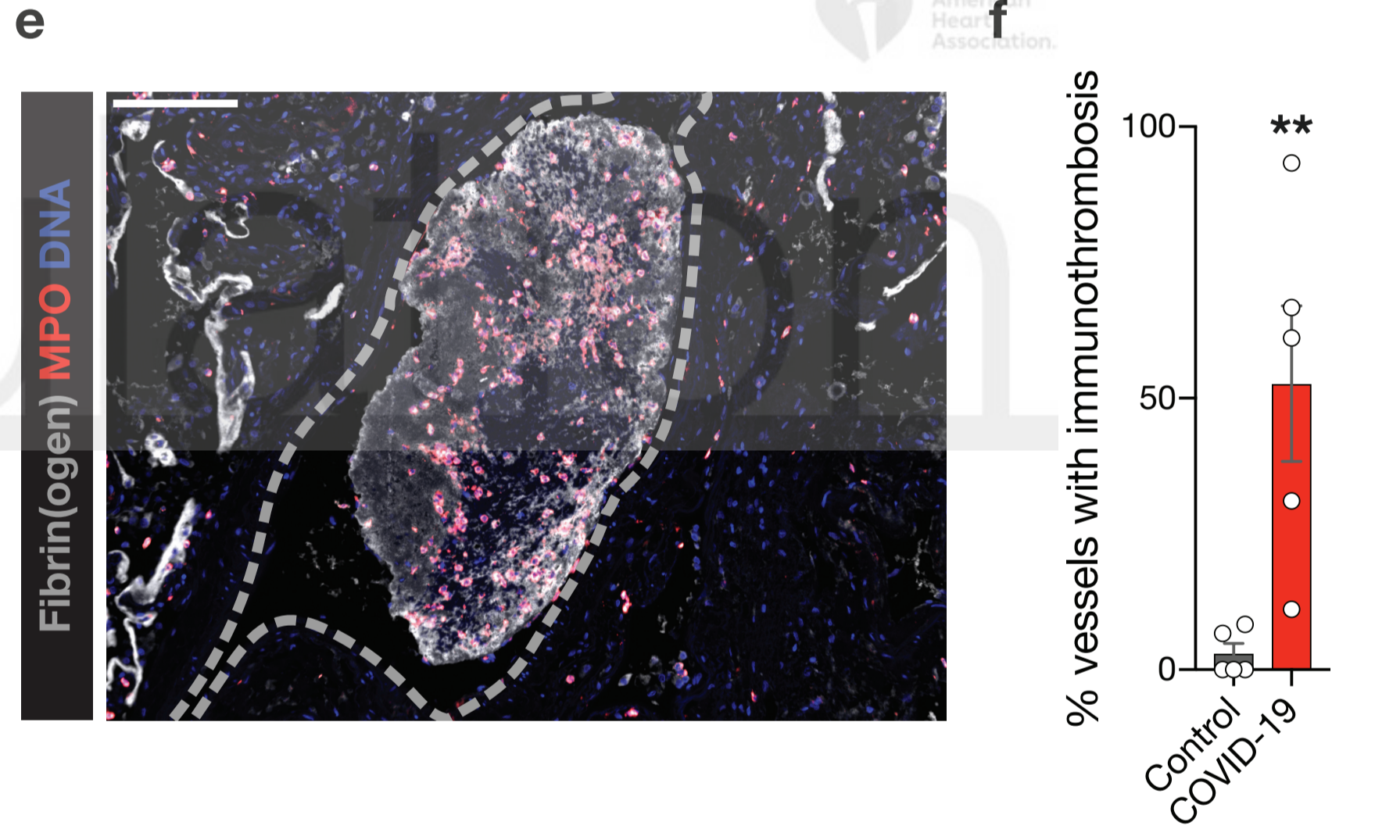
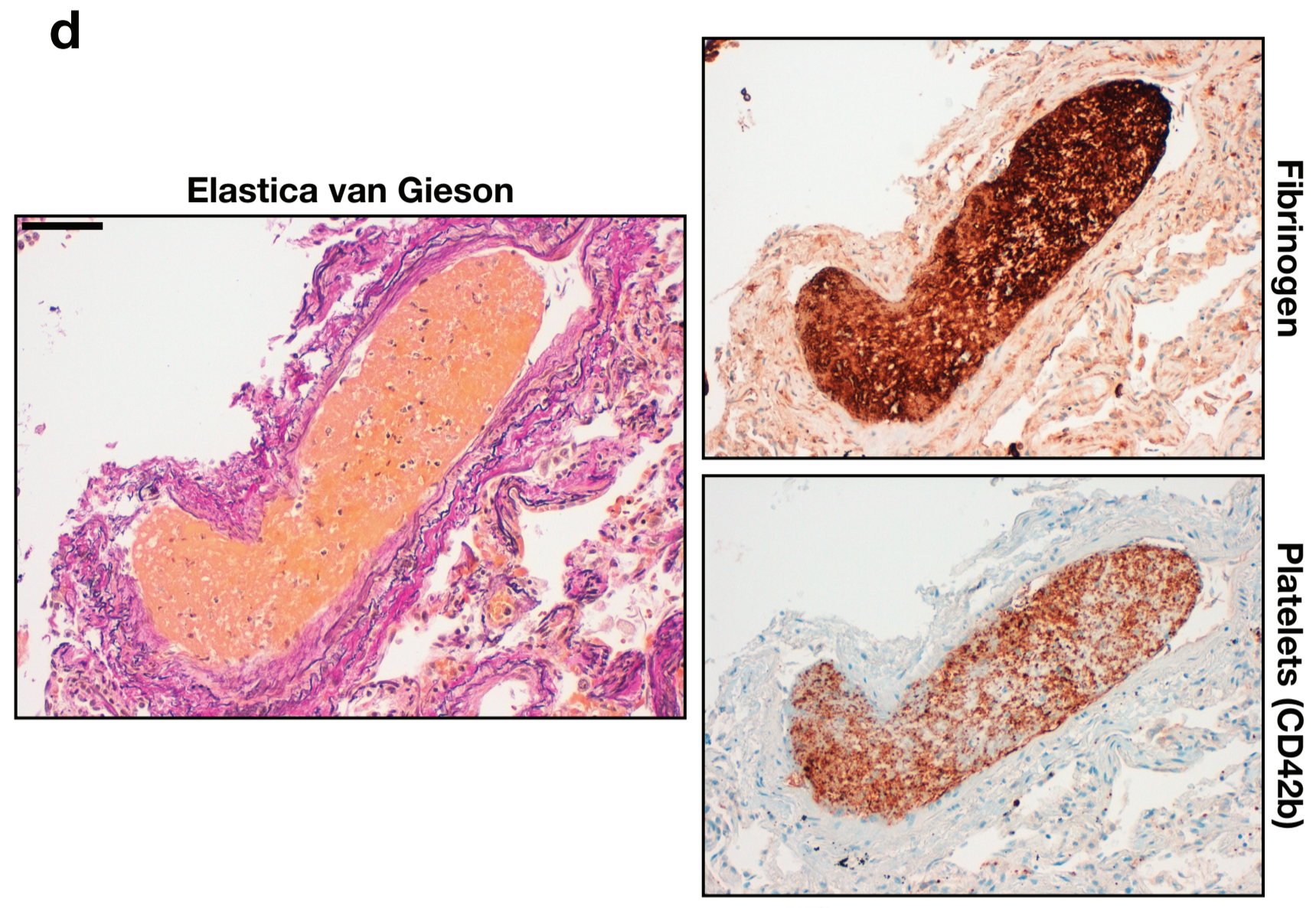
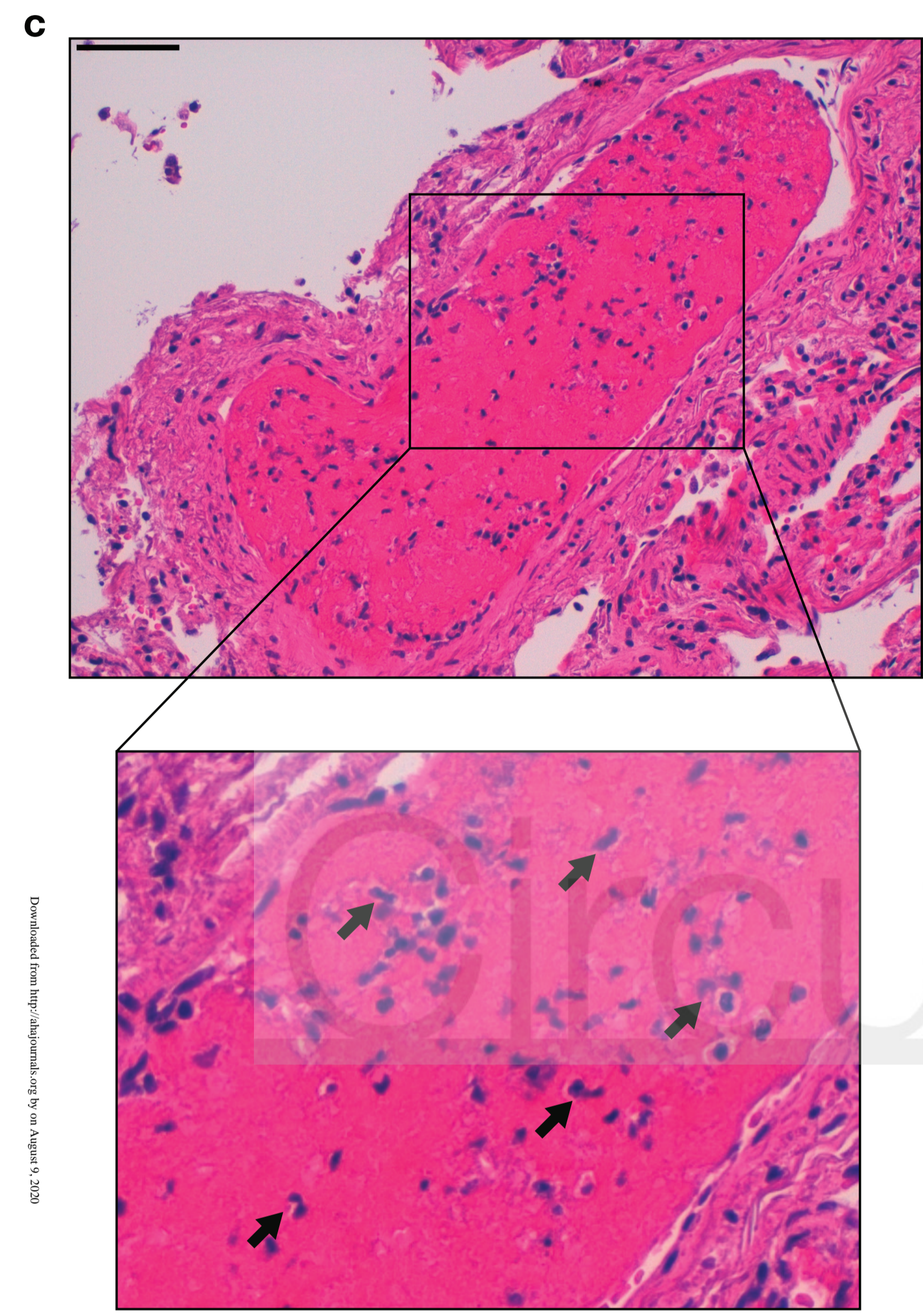
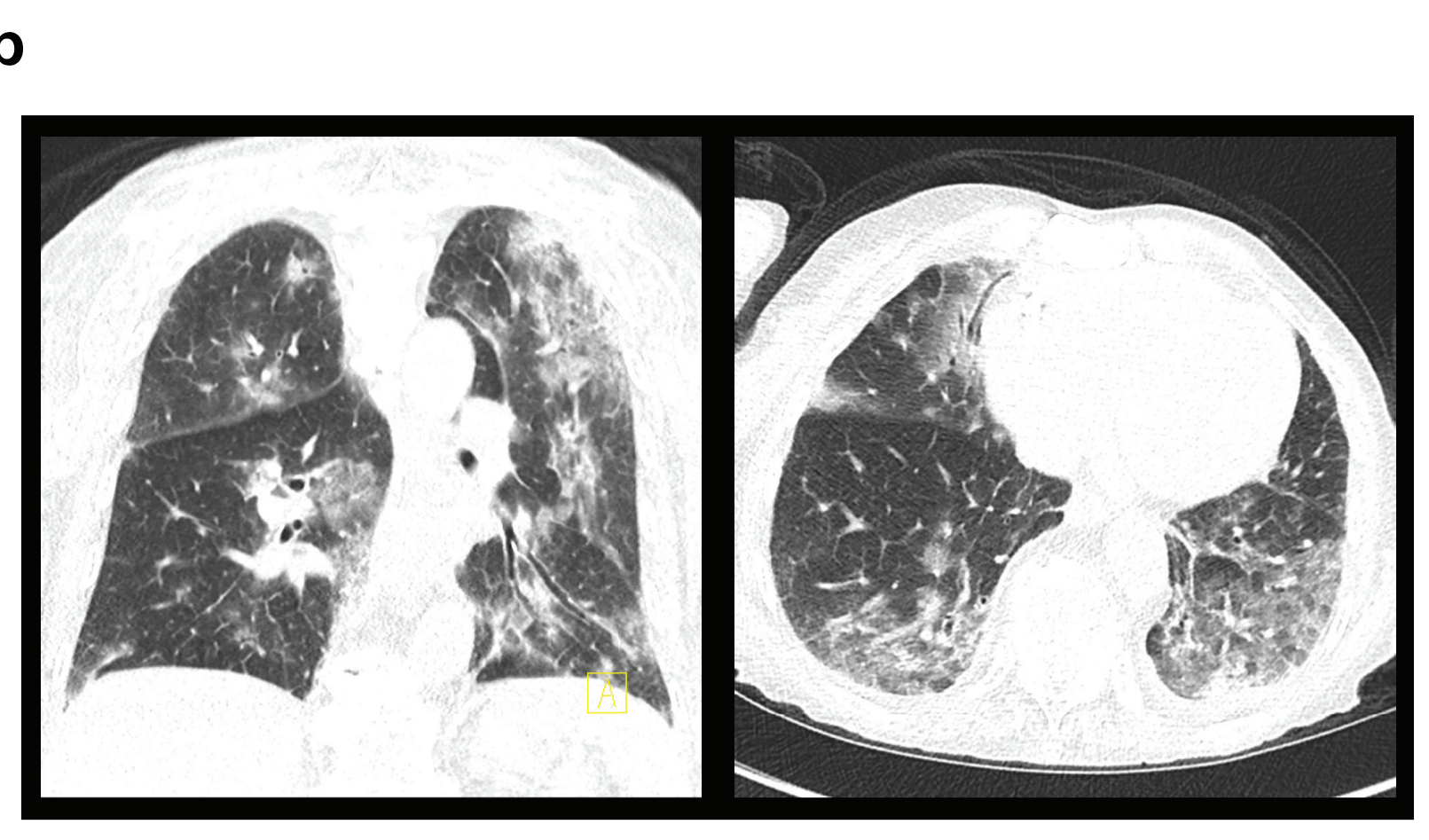
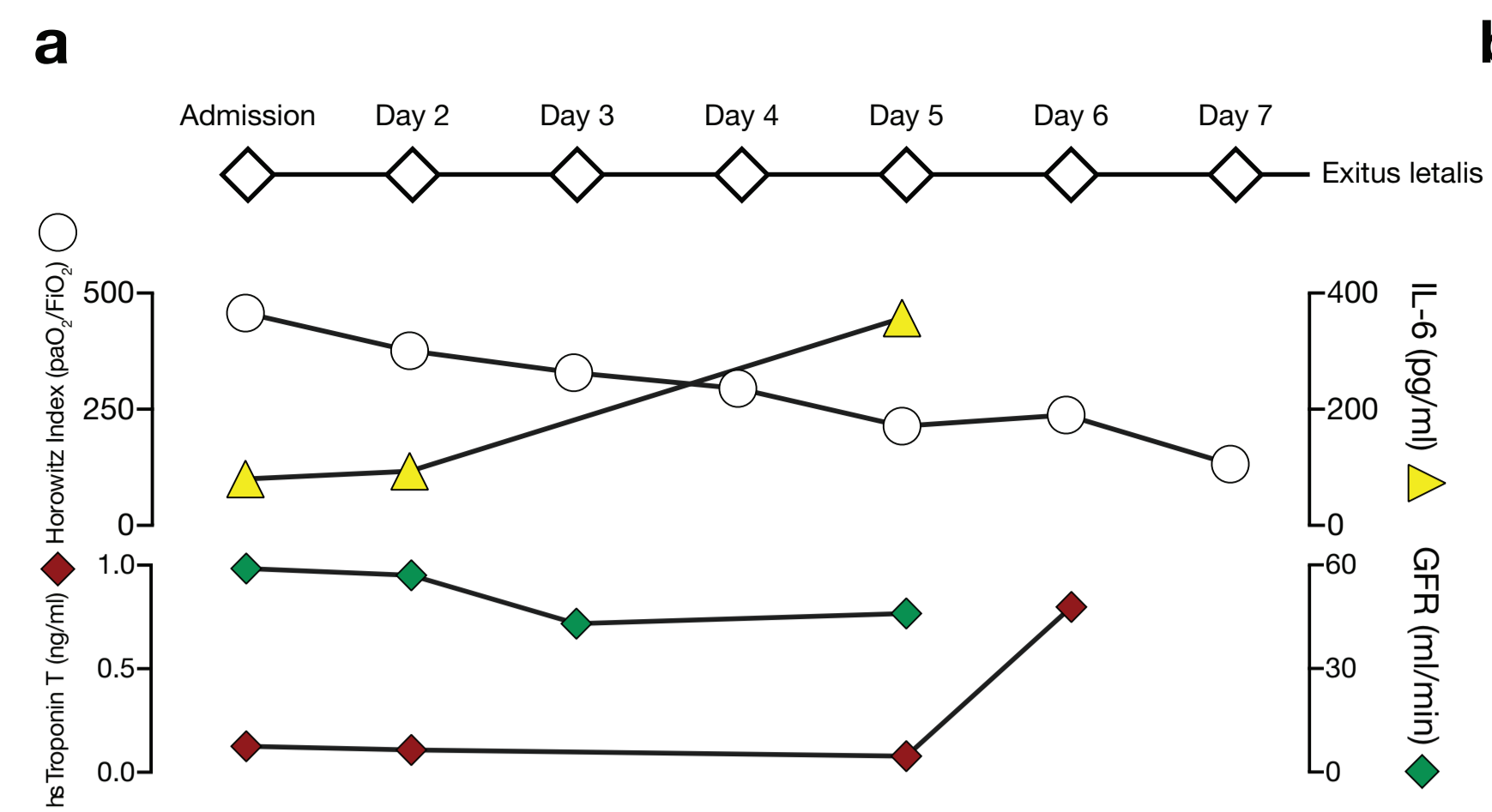
Figure 4. A systemic procoagulant state and Neutrophil extracellular trap (NET) formation in COVID-19. a, International normalized ratio (INR) and activated partial thromboplastin time (aPTT LA-sensitive) of COVID-19 patients at time of blood draw. Reference ranges are shown

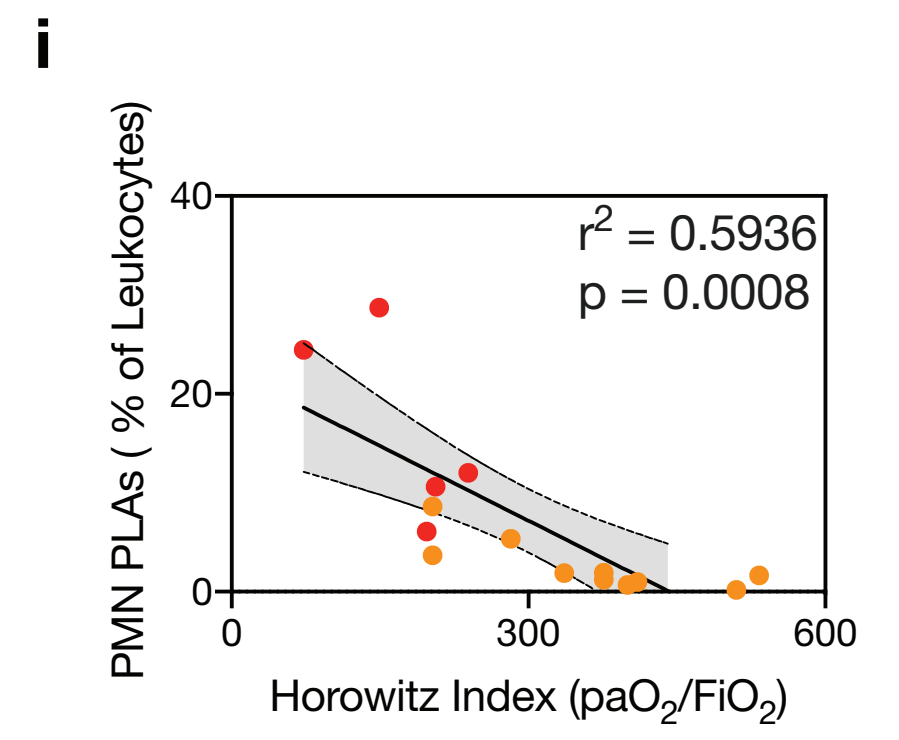
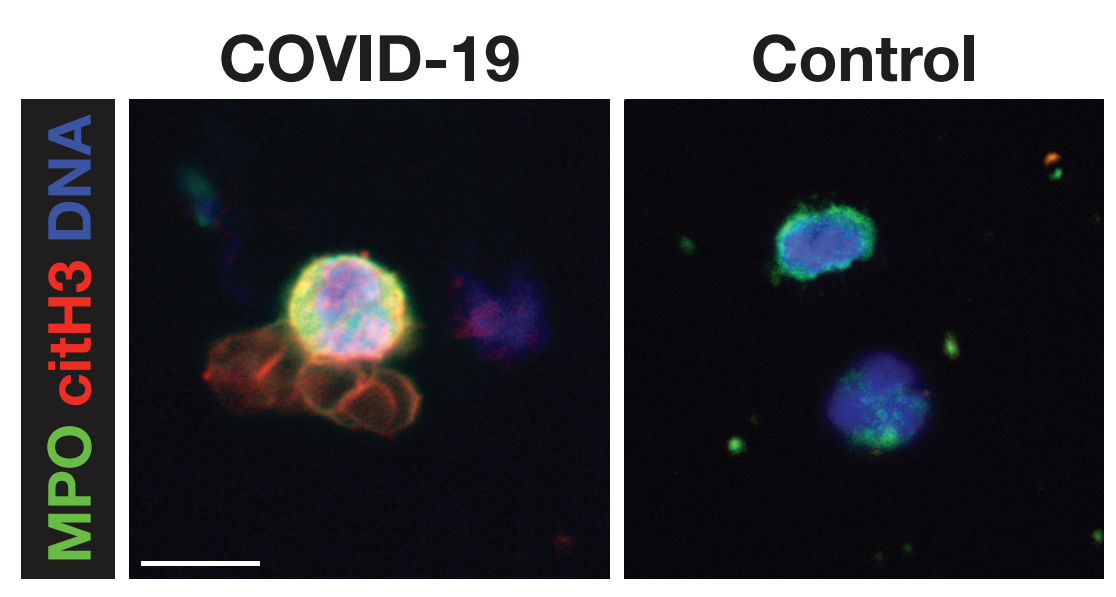
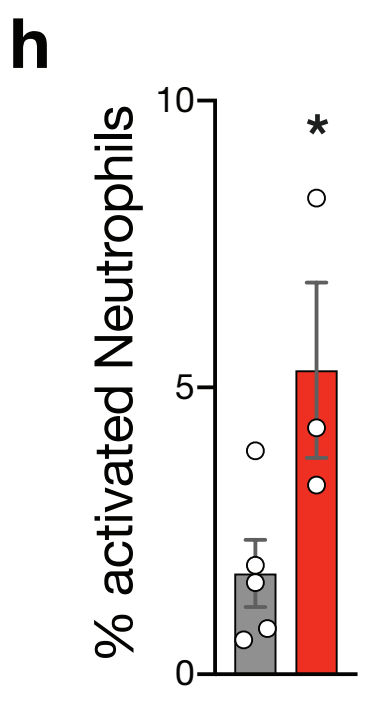
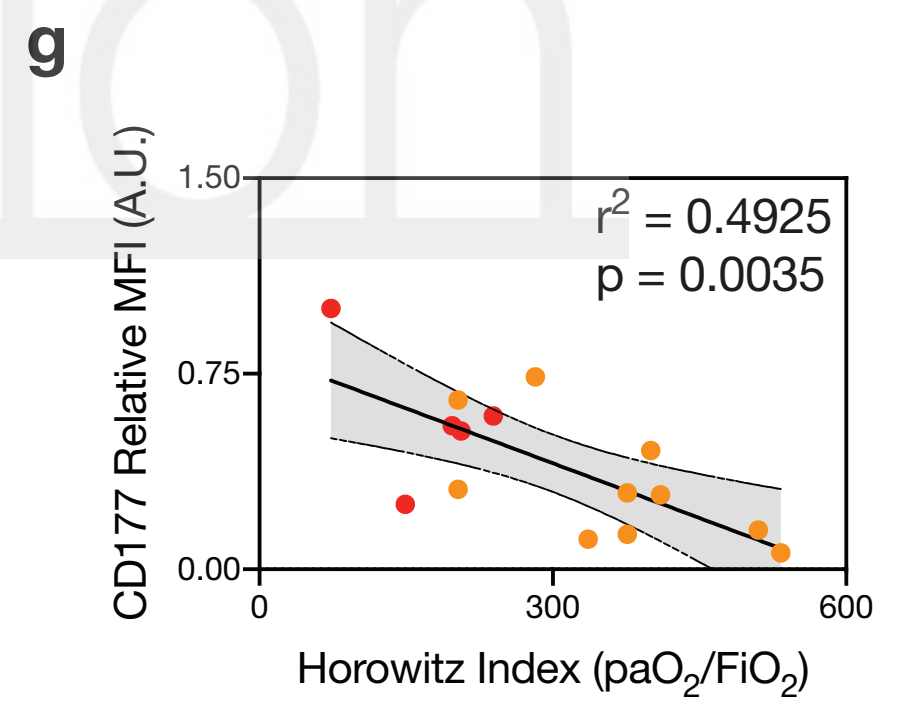
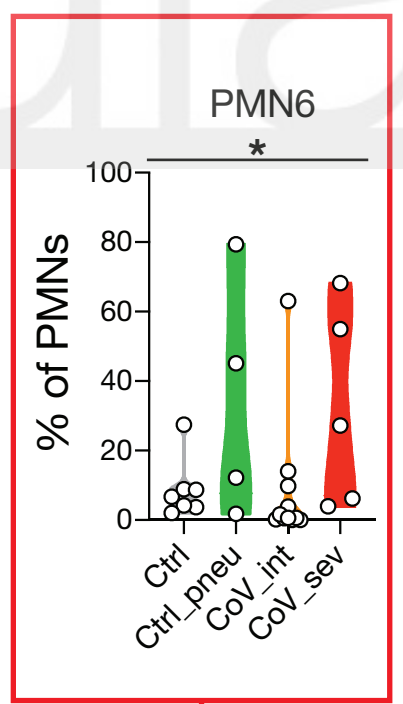
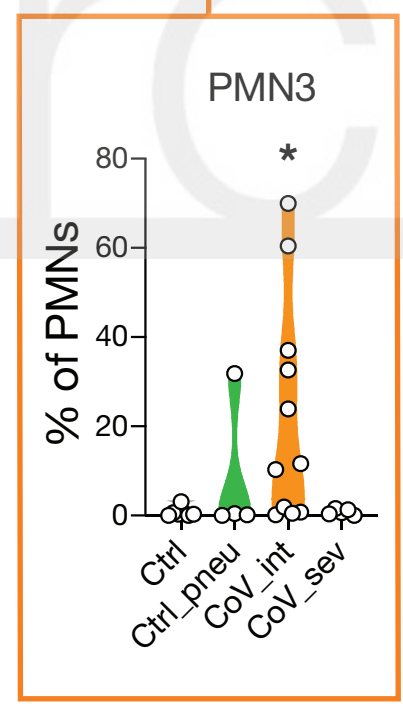
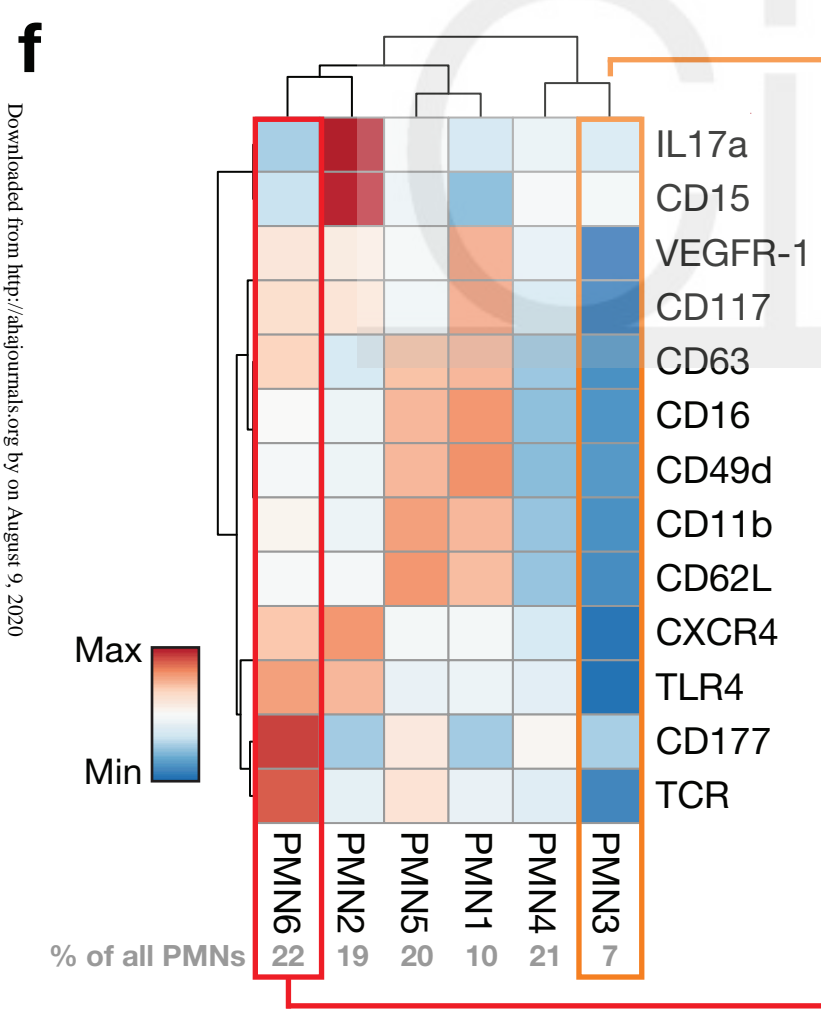
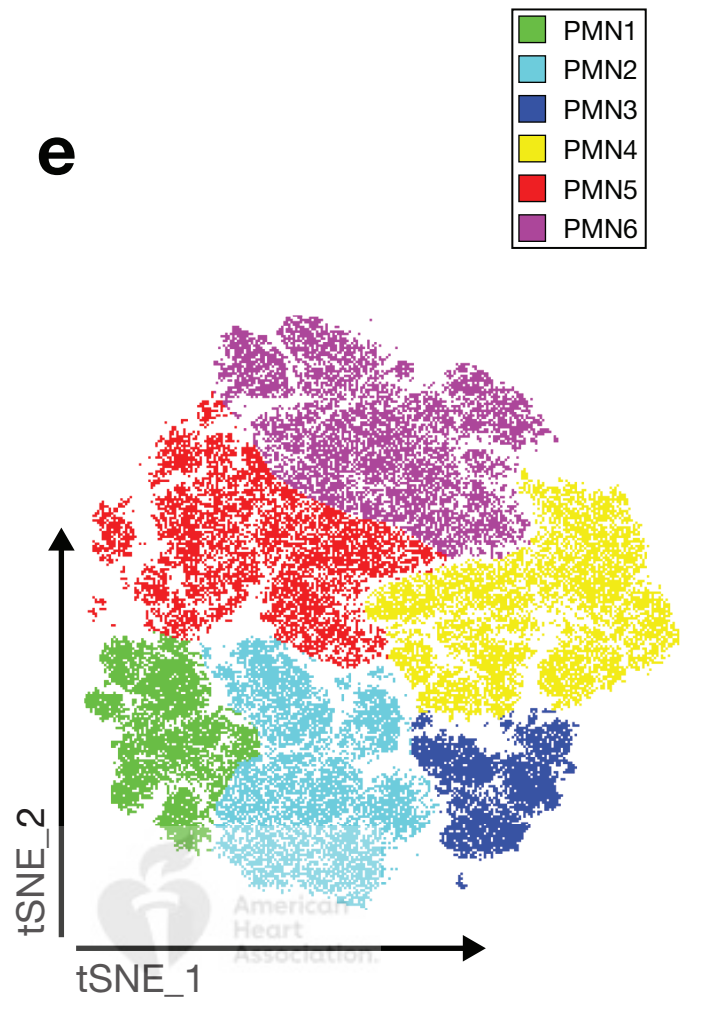
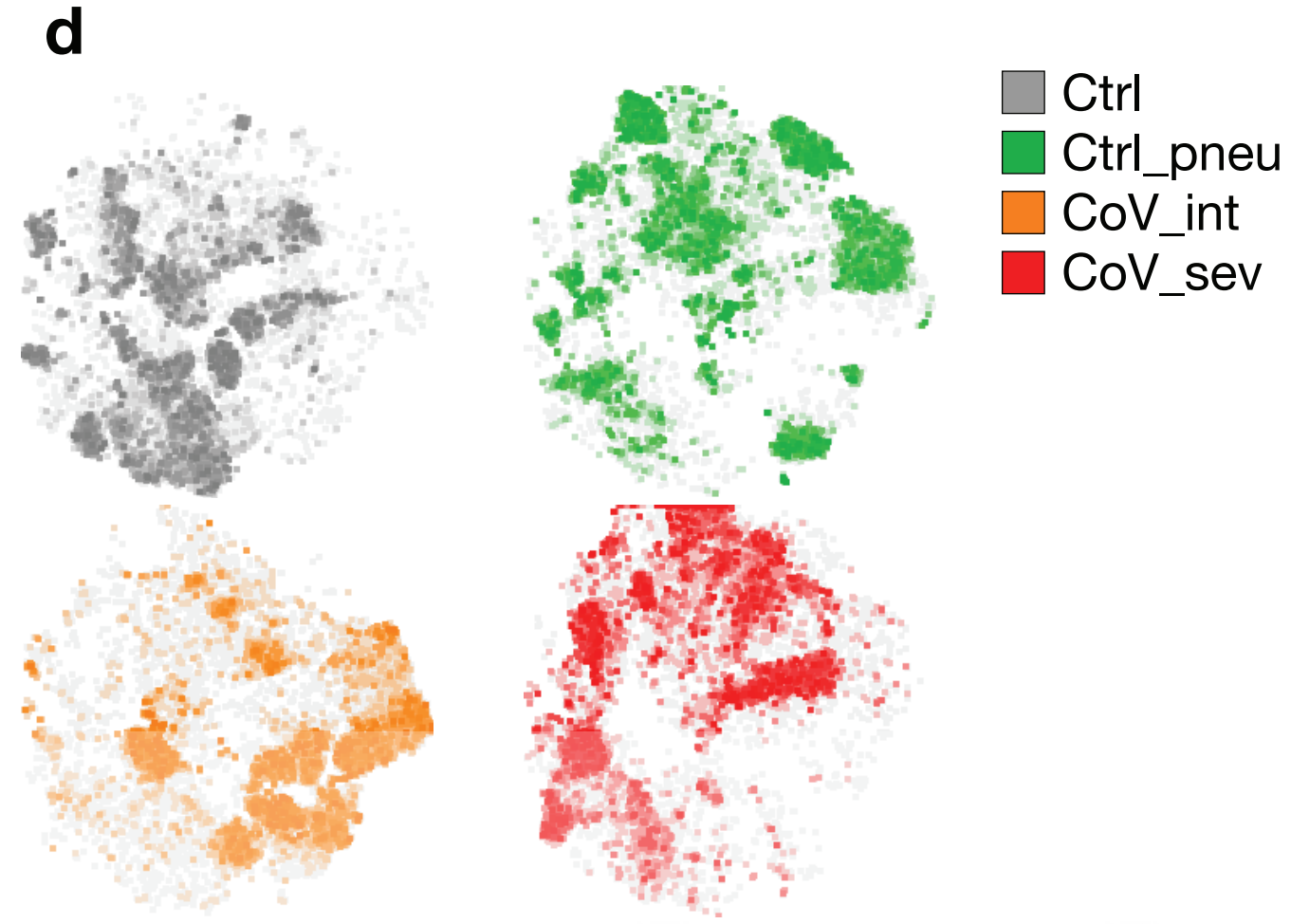
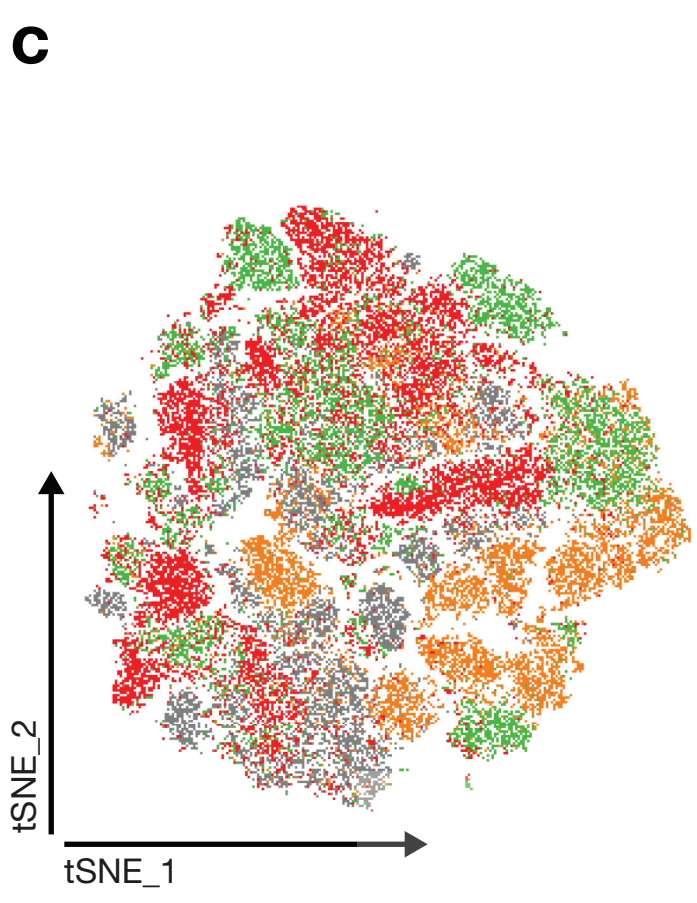
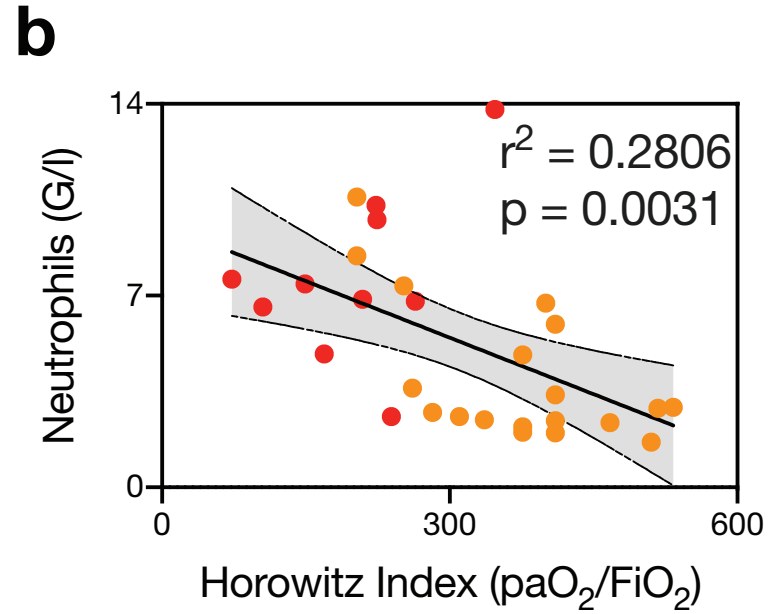
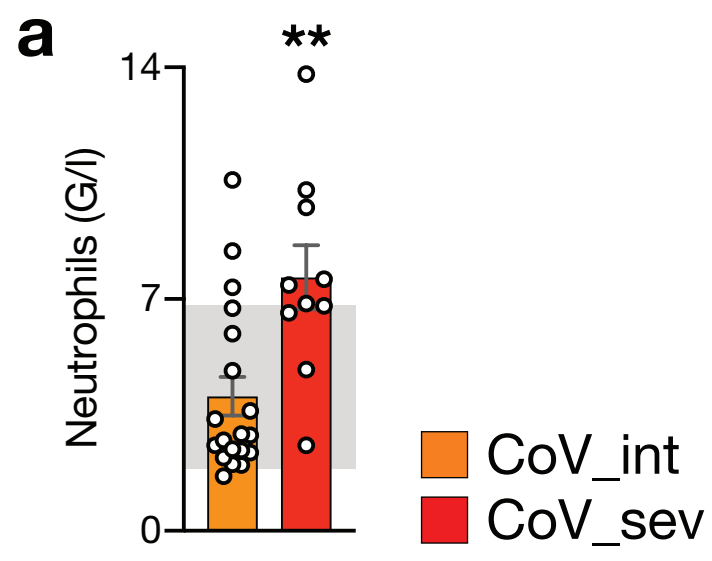
in gray (INR: 0.8-1.2, aPTT 22-34s), n=19 CoV_int, n=11 CoV_sev. **b**, Fibrinogen (Claus) plasma levels of COVID-19 patients at time of blood draw. Reference ranges are shown in gray (210-400mg/dl), n=20 CoV_int, n=11 CoV_sev. **c**, Linear regression of fibrinogen plasma level and Horowitz Index (paO₂/FiO₂) of COVID-19 patients. n=19 CoV_int (orange), n=11 CoV_sev (red). **d**, D-Dimer plasma levels of COVID-19 patients. Reference ranges are shown in gray (<0.5 µg/ml), n=20 CoV_int, n=11 CoV_sev. **e** ExTEM and InTEM Maximum Clot Firmness (MCF). Reference ranges are shown in gray (ExTEM 50-72 mm, InTEM 50-72 mm). **f**, ExTEM and InTEM Clot Formation Time (CFT). Reference ranges are shown in gray (ExTEM 34-159 mm, InTEM 30-110 mm), **g**, Linear regression of InTEM MCF and Horowitz Index. **h**, ExTEM maximum lysis (ML). Reference ranges are shown in gray (<15%), **i**, Linear regression of ExTEM ML and Horowitz Index. **j**, FibTEM MCF, Reference ranges are shown in gray (9-25 mm). **k**, Linear regression of FibTEM MCF and Fibrinogen plasma levels. e-k: CoV_int n=9 and CoV_sev n=8. **e,f,h,j**: Two-tailed unpaired Student's t-test. **l**, Schematic of the PRP-stimulation assay. **m**, Representative micrograph of platelets isolated from a CoV_sev patient binding to a neutrophil undergoing NETosis *in vitro* and quantification of control or COVID-19 platelets associated with neutrophils (see l). Scale bar: 10 µm. **n**, Representative micrographs and quantification of NETs formed by neutrophils stimulated with control or COVID-19 PRP (see l). Scale bar: 20µm. **m-n**: n=3 COVID-19 patients, n=5 controls. Two-tailed unpaired Student's t-test. **o**, Immunofluorescence staining of a representative COVID-19 lung autopsy specimen. Arrow: activated neutrophil, Stars: Neutrophil extracellular traps. top right: 3D reconstruction of NETing neutrophil, Arrow indicates citH3 and DNA signal in MPO+ NET structure. Bottom right: pseudocolored Fibrinogen co-staining. Scale bar: 10 µm, dashed lines indicate vessel borders. **p**, NETs per vessels of COVID-19 and non-COVID-19 lung autopsy specimens. n=5

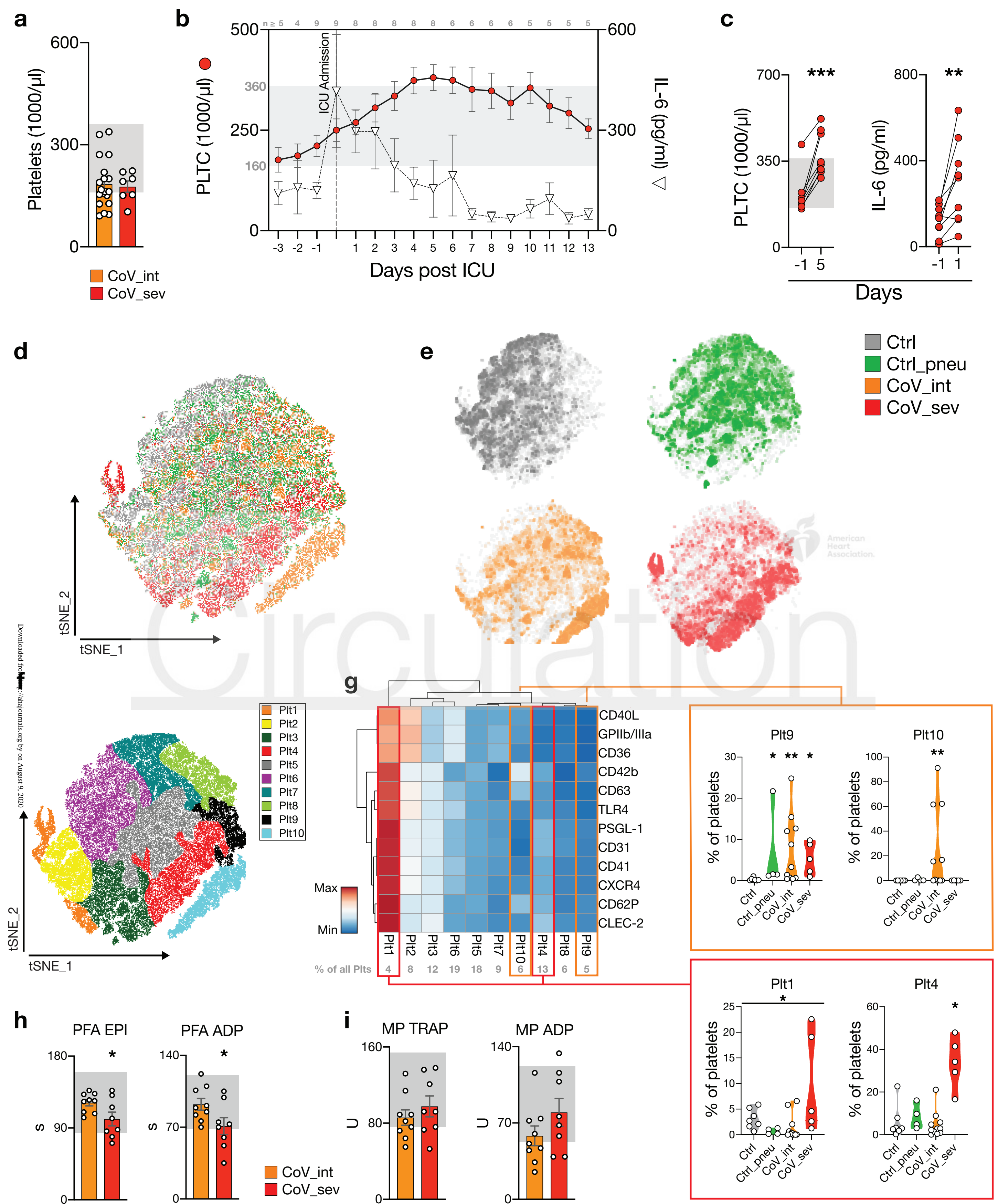
COVID-19 patients, n=5 controls. Two-tailed unpaired t-test with Welch's correction. **q**, Immunofluorescence staining of COVID-19 autopsy specimens of the lung, kidney and heart. Top: Staining for neutrophils (Myeloperoxidase, MPO), DNA, and citrullinated Histone H3 (citH3). Rectangles show areas of interest with NET-like structures in all three organs that are enlarged in Fig. 4r. Bottom: Fibrinogen staining is pseudocolored. Scale bar: 10 μm , dashed lines indicate vessel borders. **r**, Enlarged areas from q with NET-like structures (arrows). Scale bar: 10 μm . * $p < 0.05$, ** $p < 0.01$, *** $p < 0.001$.

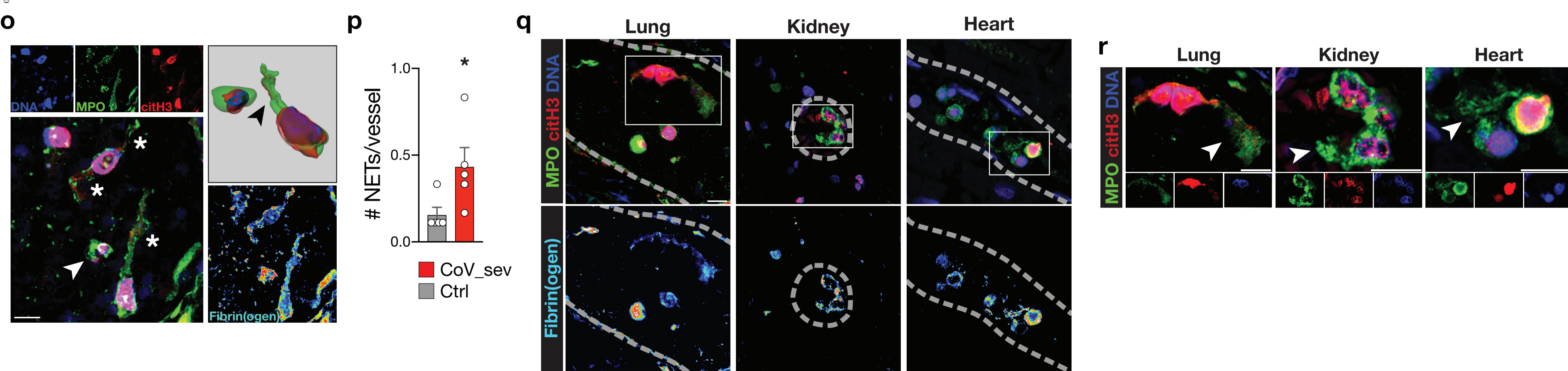
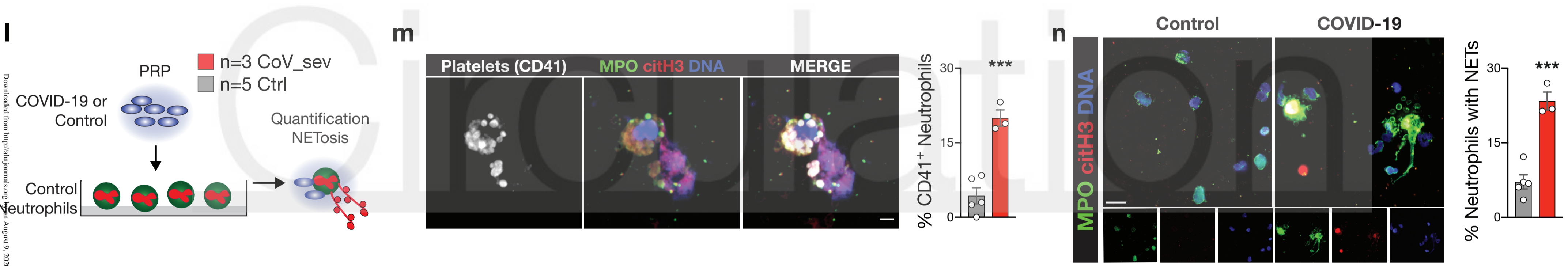
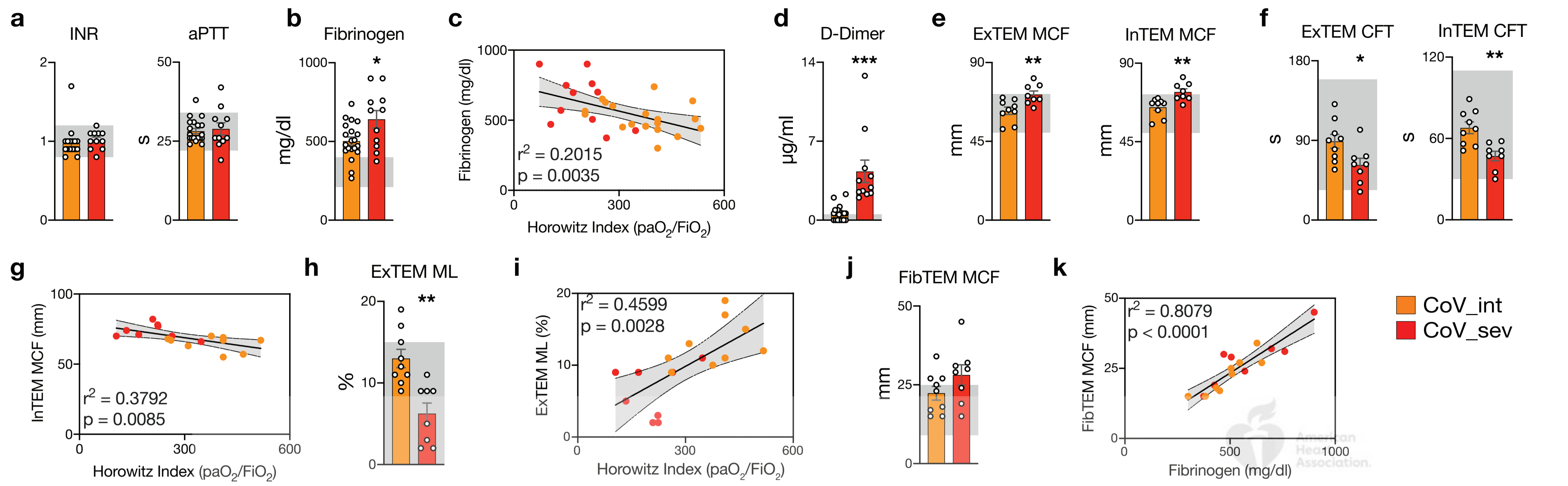


Circulation









Downloaded from <http://ahajournals.org> on August 9, 2020